CarbonTracker-CH_4: An assimilation system for estimating emissions of atmospheric methane

L. Bruhwiler[1], E. Dlugokencky[1], K. Masarie[1], M. Ishizawa[2], A. Andrews[1], J. Miller[1], C. Sweeney[1], P. Tans[1], D. Worthy[4]

[1]{NOAA Earth System Research Laboratory, Global Monitoring Division, Boulder Colorado, USA}

[2]{National Institute for Environmental Studies, Center for Global Environmental Research, Tsukuba, Japan}

[4]{Environment Canada, Climate Research Division, Toronto, Ontario, Canada}

Correspondence to: L. M. Bruhwiler (lori.bruhwiler@noaa.gov)

Abstract

We describe an assimilation system for atmospheric methane (CH_4), CarbonTracker-CH_4, and demonstrate the diagnostic value of global or zonally averaged CH_4 abundances for evaluating the results. We show that CarbonTracker-CH_4 is able to simulate the observed zonal average mole fractions and capture inter-annual variability in emissions quite well at high northern latitudes (53-90N). In contrast, CarbonTracker-CH_4 is less successful in the tropics where there are few observations and therefore misses significant variability and is more influenced by prior flux estimates. CarbonTracker-CH_4 estimates of total fluxes at high northern latitudes are about 81 ± 7 Tg CH_4 yr^{-1}, about 12 Tg CH_4 yr^{-1} (13%) lower than prior estimates, a result that is consistent with other atmospheric inversions. Emissions from European wetlands are decreased by 30%, a result consistent with previous work by Bergmaschi et al. (2005); however, unlike their results, emissions from wetlands in Boreal Eurasia are increased relative to the prior estimate. Although CarbonTracker-CH_4 does not estimate an increasing trend in emissions from high

northern latitudes for 2000 through 2010, significant inter-annual variability in high northern latitude fluxes is recovered. Exceptionally warm growing season temperatures in the Arctic occurred in 2007, a year that was also anomously wet. Estimated emissions from natural sources were greater than the decadal average by 4.4 ± 3.8 Tg CH_4 yr^{-1} in 2007.

CarbonTracker-CH_4 estimates for temperate latitudes are only slightly increased over prior estimates, but about 10 Tg CH_4 yr^{-1} is redistributed from Asia to North America. This difference exceeds the estimated uncertainty for North America (± 3.5 Tg CH_4 yr^{-1}). We used time invariant prior flux estimates, so for the period from 2000 to 2006, when the growth rate of global atmospheric CH_4 was very small, the assimilation does not produce increases in natural or anthropogenic emissions in contrast to bottom-up emission datasets. After 2006, when atmospheric CH_4 began its recent increases, CarbonTracker-CH_4 allocates some of the increases to anthropogenic emissions at temperate latitudes, and some to tropical wetland emissions. For temperate North America the prior flux increases by about 4 Tg CH_4 yr^{-1} during winter when biogenic emissions are small. Examination of the residuals at some North American observation sites suggests that increased gas and oil exploration may play a role since sites near fossil fuel production are particularly hard for the inversion to fit and the prior flux estimates at these sites are apparently lower and lower over time than what the atmospheric measurements imply.

The tropics are not currently well resolved by CarbonTracker-CH_4 due to sparse observational coverage and a short assimilation window. However, there is a small uncertainty reduction and posterior emissions are about 18% higher than prior estimates. Most of this increase is allocated to tropical South America rather than being distributed among the global tropics. Our estimates for this source region are about 32 ± 4 Tg CH_4 yr^{-1}, in good agreement with the analysis of Melack et al. (2004) who obtained 29 Tg CH_4 yr^{-1} for the most productive region, the Amazon Basin.

1 Introduction

Methane (CH_4) is second in importance to carbon dioxide (CO_2) among greenhouse gases with significant anthropogenic sources. It has a radiative forcing of, 0.5 ± 0.05 Wm^{-2}, about 28% that of non-CO_2 atmospheric constituents in 2010 (Hofmann et al, 2006; updated at http://www. esrl.noaa.gov/gmd/aggi/). Over a 100-year time horizon CH_4 is 28 times more efficient per mass as a greenhouse gas than CO_2 (Myhre et al., 2013).

Global emissions of CH_4 are between 500 and 600 Tg CH_4 yr^{-1} (Kirschke et al, 2013 and this work) and about 40% of this is due to natural sources, mainly wetlands. The other 60% of global emissions are due to microbial emissions associated with rice agriculture, livestock and waste, and fugitive emissions from fossil fuel production and use (Denman et al., 2007). Global emissions have recently been approximately in balance with global sinks, mainly chemical destruction by reaction with OH, but also from oxidation by soil microbes, and atmospheric reactions with O^1D and Cl in the stratosphere. The lifetime of CH_4 in the atmosphere is about 10 yr (e.g. Dlugokencky et al., 2003) with CO_2 the eventual product of its oxidation.

CH_4 has increased from a preindustrial abundance of 722 ± 4 ppb (Etheridge et al., 1998 after conversion to the NOAA 2004 CH_4 standard scale (Dlugokencky et al., 2005)) to current values of about 1800 ppb in 2010 (about 2.5 times), and it is likely that human activity is responsible for most of this increase. Current levels are unprecedented over at least the last 800 kyr (Loulerge et al., 2008). NOAA atmospheric network observations extend back to the 1980s, and show that global CH_4 increased rapidly through the late 1990s, leveled off during the early 2000s and have recently begun to increase since 2007 (Rigby et al., 2008; Dlugokencky et al., 2009). The subject of the causes of the recent increase is the topic of much recent work (e.g. Bousquet et al., 2011), including this study.

An important aspect of atmospheric CH_4 is the sensitivity of natural wetland emissions to climate change. Emissions from the Arctic, in particular, have the potential to increase significantly as temperatures rise and the vast stores of soil carbon thaw (e.g. Schuur et al., 2011; Harden et al., 2012). Schaefer et al. (2010) pointed out that potential carbon emissions from the Arctic could have important implications for policies aimed at reducing or stabilizing emissions. This clearly highlights the importance of maintaining long-term measurements of atmospheric CH_4 in the Arctic, and in this study we hope to further the case for atmospheric inverse techniques as a tool to diagnose observed atmospheric records (see previous studies by Hein et al., 1997; Houweling et al., 1999; Chen and Prinn, 2006; Bergamaschi et al., 2005; Bousquet et al., 2006; Bergamaschi et al, 2013; Houweling et al., 2013).

Atmospheric CH_4 is also influenced by diverse human activities, ranging from food production (ruminants and rice) to waste (sewage and landfills) to fossil fuel production (coal, oil and gas). Future increases in population could increase emissions from agriculture and waste as demand for more food production rises, while the current boom in shale oil/gas exploitation has focused attention on leakage from drilling, storage and transport of fossil fuel (e.g. Pétron et al., 2012). An obvious use of an atmospheric assimilation system is to quantify changes in anthropogenic emissions and attribute increases at policy relevant spatial scales, something that is possible only with adequate spatial coverage of observations. In this study we will discuss the degree to which this is currently possible given the coverage of the current observational network.

The work we present here uses only surface observations rather than combinations of surface observations and retrievals space-based instruments as used by Bergamaschi et al. (2013) and Houweling et al. (2014). Our study differs from that of Bergmaschi et al. (2013) since they used a subset of 30 surface observations sampling mainly background marine air that existed over the entire decade, as well as satellite retrievals. In our study we have used most available surface observations, including those that are sensitive to terrestrial emissions (Table 2). We use the same transport model as Bergamaschi et al. (2013) and Houweling et al. (2014), however, we use a different assimilation technique and different strategies for weighting observations and priors. We also include a discussion of observationally derived quantities that useful evaluation of our results.

The next section is a detailed description of our CH_4 assimilation system, CarbonTracker-CH_4, followed by a detailed evaluation of its performance. In section 4, we discuss results from CarbonTracker-CH_4 for 2000-2010.

2 The CarbonTracker Ensemble Data Assimilation System

The total emission of CH_4 in time and space may be described by:

$$F(x, y, t) = \lambda_1 \; F_{natural}(x, y, t) + \lambda_2 \bullet F_{fossil}(x, y, t) + \lambda_3 \bullet F_{agriculture/waste}(x, y, t) + \lambda_4 \bullet F_{fire}(x, y, t) + \lambda_5 \bullet F_{ocean}(x, y, t)$$

Where λ_i represents a set of linear scaling factors to be estimated in the assimilation that are applied to the fluxes (F) by multiplying prior estimates of CH_4 fluxes to produce the posterior flux estimates. The prior values of the scaling factors is 1. A total of 121 parameters per week are estimated; 10 terrestrial emission processes for 12 continental regions (corresponding to the Transcom 3 continental regions (Gurney et al., 2000) but with the addition of a tropical African region, see http://transcom.project.asu.edu for a map, or Fig. 1), and fluxes from the global ocean. Each weekly assimilation step, emissions for the previous 5 weeks are estimated following the fixed lag Kalman smoother methodology described by Bruhwiler et al., (2005). The terrestrial emissions include fugitive emissions from coal, oil and gas production (estimated as one source); agriculture and waste emissions (rice production, for example); livestock and their waste; and emissions from landfills and wastewater. Natural emissions include contributions from wetlands, termites, uptake in soils and wild animals. The final terrestrial emission category is biomass burning, which is treated as a separate category due to the existence of strong spatial constraints coming from satellite observations of locations of large fires. In general, the spatial distribution of the prior flux estimates is an important constraint on the assimilation. For example, the known location of fossil fuel production from bottom-up emission data sets provides information to the assimilation system on whether a signal measured at a particular observation site could have a fossil fuel component. If production areas change over time and not captured by the prior distribution, then fossil fuels will be underestimated by the inversion.

In this study we estimate emissions for continental scale source regions, and although we rely on the prior spatial distribution of the prior emissions to distribute the emissions, the use of large source regions can lead to aggregation errors as shown by Kaminski et al. (2001). An alternative would be to solve for many more sources, possibly at grid scale. However, without significantly more observational constraints, our solution would be very dependent on not only the prior emissions, but also their assumed spatial and temporal covariance. Ultimately, use of space-based observations might be the preferred solution. At present, significant issues with space-based emissions still exist, such as quantification of biases that vary with space and time (e.g. Houweling et al., 2013). On the other hand, as discussed by Bruhwiler et al. (2011), the global network can constrain certain aspects of the budgets of greenhouse gases, even with its bias towards background atmospheric sites.

We initialized the assimilation using an equilibrated distribution produced by a previous TM5 run that was scaled to match observed zonal average CH_4 mixing ratio for the year 2000. The north-south gradient therefore should represent the observed atmospheric gradient at the surface. Sensitivity runs using synthetic data (not shown) suggest that spin-up effects are restricted to within in the first half year of the assimilation.

2.1 Ensemble Size and Localization

The ensemble Kalman smoother system used to solve for the scalar multiplication factors is based on that described by Peters et al. (2005), and uses the square root ensemble Kalman filter of Whitaker and Hamill (2002). The length of the smoother window is restricted to five weeks for computational efficiency. Although the posterior flux estimates in relatively densely sampled regions such as North America were found to be robust by Peters et al. (2005) with a window this short, regions with less dense observational coverage (the tropics, for example) are likely to be poorly constrained even after more than a month of transport and therefore not well resolved. As pointed out by Bruhwiler et al. (2005), a smoother window of at least 3 months is likely to make maximal use of remote network sites, however this may come at the expense of accumulated errors in transport as claimed by Peters et al. (2007). The extent to which this is true is a subject for further study. Even without the problem of a short smoother window, the sparseness of the observational network makes it difficult to resolve under-sampled regions such as the tropical terrestrial biosphere (Bruhwiler et al., 2011).

Statistics for the ensemble are created from 500 members using the prior covariance matrix of the parameters, each with its own background CH_4

concentration field to represent the time history (and thus covariances) of the filter. We experimented with different numbers of ensemble members and found that the use of too few ensemble members results in solutions that stay artificially close to prior flux estimates. To dampen spurious noise due to the approximation of the covariance matrix, we apply localization (Houtekamer and Mitchell, 1998) for non-background sites. By limiting correlations between distant sites, localization ensures that random correlations between parameters do not translate into unrealistic constraints on emissions by distant measurement sites (i.e. those connections physically impossible with only 5 weeks of transport). Following Peters (2005) localization is based on the linear correlation coefficient between the 500-parameter deviations and 500 observation deviations for each parameter, with a cut-off at 95% significance in a student's t-test with a two-tailed probability distribution.

As noted above, the posterior covariance matrix is approximated by using the posterior parameter deviations. Temporal covariance is limited to the period spanned by the assimilation window. Therefore, time aggregated quantities, such as annual uncertainties will likely be overestimates since information about temporal covariations will be limited. Furthermore, as with any inversion, the error covariance matrix ultimately reflects the relative weighting between the model-data mismatch errors and prior emission uncertainties that are specified.

2.2 Covariance Structure

In our assimilation, the chosen 1-σ error of the prior estimates is 75% for all parameters. The prior covariance structure describes the uncertainty on each parameter, plus their correlation in space. For the current version of CarbonTracker-CH_4, we assumed a diagonal prior covariance matrix so that no prior correlations between estimated parameters exist. The effect of this choice may be strong anti-correlations among estimated parameters in regions where few observational constraints exist; however, larger-scale aggregations of these regions are expected to yield more robust estimates. For example, the total tropical source can be better determined that the individual regions between which there can be trade-offs in emissions from time step to time step. Note also that the 5-week assimilation window used by CarbonTracker limits knowledge of temporal correlations. As a result, the uncertainty on annual average emissions is difficult to estimate.

2.3 TM5 Atmospheric Transport Model

Transport Model 5 (TM5, Krol et al, 2005) is a community supported global model with two-way nested grids. For CarbonTracker-CH_4, we ran the simulation at 4^o latitude x 6^o longitude resolution without zoom regions. TM5 is developed and maintained jointly by the Institute for Marine and Atmospheric Research Utrecht (IMAU, The Netherlands), the Joint Research Centre (JRC, Italy), the Royal Netherlands Meteorological Institute (KNMI, The Netherlands), and NOAA ESRL (USA). TM5 has detailed treatments of advection, convection (deep and shallow), and vertical diffusion in the planetary boundary layer and free troposphere. The winds used for transport in TM5 come from the European Center for Medium range Weather Forecast (ECMWF) operational forecast model. This "parent" model currently runs with ~25 km horizontal resolution and 60 layers in the vertical prior to 2006 and 91 layers in the vertical from 2006 onwards.

The ECMWF meteorological data are preprocessed into coarser grids and are converted from wind fields to mass conserving horizontal and vertical mass fluxes. TM5 runs at an external time step of three hours, but due to the symmetrical operator splitting between advection, diffusion, emissions and loss the effective time step over which each process is applied is shorter. The vertical resolution of TM5 used with CarbonTracker-CH_4 is 34 hybrid sigma-pressure levels (from 2006 onwards; 25 levels for 2000-2005), unevenly spaced with more levels near the surface.

2.4 Prior Emission Estimates for Natural Sources

The largest natural emissions of methane are from wetlands, defined as regions that are permanently or seasonally water logged. Wetlands are a broad category that includes both high-latitude bogs and fens and tropical swamps. Saturated soils in warm tropical environments tend to produce the most methane. However, warming Arctic temperatures raise concerns of increasing output from high-latitude wetlands and future decomposition of carbon currently stored in frozen Arctic soils (e.g. Schaefer et al., 2011).

Methane is rapidly oxidized by methanotrophic bacteria in overlying aerobic water columns or unsaturated soil, so the water table must be at or near the surface and the depth of overlying water must be shallow for large emissions to occur. Wetland plants have adapted to low oxygen environments by having hollow stems to allow delivery of oxygen and other gases to root systems. These hollow stems also allow delivery of methane directly to the atmosphere, and along with ebullition account for most of transport to the atmosphere. Diffusion also occurs but is a significantly smaller contribution to the atmosphere. (See Barlett and Harris (1993) for an extensive overview of wetland emissions.) Bottom-up estimates of global emissions from wetlands are about 150-200 Tg CH_4 yr^{-1} with most of this occurring in tropical regions (Melton et al., 2013). Because emissions are sensitive to temperature and precipitation, they exhibit significant seasonal cycles, especially at high latitudes, as well as inter-annual variability due to moisture and temperature variability.

Methane emissions from wetlands are difficult to quantify using assimilation systems for two reasons; their global spatial distribution is difficult to know accurately, and there is large variability in emission rates over small spatial scales (meters), which makes extrapolation to large scales difficult. Here we used the prior flux estimates of Bergamaschi et al. (2005) that are based on the wetland distribution of Matthews and Fung (1989) and the wetland emission model of Kaplan (2002) that parameterizes emissions based on moisture, temperature and soil carbon. The global total of the prior flux estimate is 175 Tg CH_4 yr^{-1}.

Other natural sources of methane include enteric fermentation in insects (mainly termites, Sanderson (1996)) and wild ruminants (Houweling et al.,1999). Prior values for both of these sources (~ 25 Tg CH_4 yr^{-1}) are much smaller than the wetland source. Oxidation of CH_4 in dry soils (~40 Tg CH_4 yr^{-1}, Ridgwell et al. (1999)) is a natural sink of CH_4 and is treated as a negative source in the assimilation.

2.5 Prior Emission Estimates for Fugitive Emissions from Fossil Fuels

Methane is the principal component of natural gas, and leaks to the atmosphere associated with natural gas production and distribution are a considerable source. Natural gas is associated with oil production and is often flared, or simply vented to the atmosphere. Together, anthropogenic emissions from oil and gas production are thought to contribute about 50 Tg CH_4 yr^{-1} (~10% of the global annual methane emissions, EDGAR 3.2FT2000 (European Commission, JRC, 2009). Methane is also associated with coal deposits and can be released by extracting and pulverizing coal. It is often vented directly to the atmosphere from mines, and this source contributes an additional ~20 Tg CH_4 yr^{-1} (EDGAR 3.2FT2000 (European Commission, JRC, 2009). As Asian economies have undergone rapid growth, coal production there has increased by a factor of about two since 2000, while remaining approximately level for most of the rest of the world. In 2010, production of coal by China increased by 9% over the previous year (BP Statistical Energy Review, 2011).

Combustion of natural gas is currently used to generate about a quarter of the electricity produced in the U.S. Its popularity as a fuel has recently grown because it is a relatively clean and efficient source of energy. Recent technological advances in recovery of natural gas, principally hydraulic fracturing, have led to increases in reserve estimates, and a tremendous increase in exploitation of shale oil/gas deposits in North America (e.g. Energy Information Administration; http://www.eia.gov). It is possible that as natural gas reserves are increasingly exploited, emissions related to its production and distribution will rise in the future.

CarbonTracker-CH_4 uses the 1°x1° gridded emissions from EDGAR 3.2FT2000 (European Commission, JRC, (2009) as prior emission estimates for fugitive emissions from coal, oil and gas production. This data set is based on emission inventories by country and sector for 1990 and 1995 extrapolated to 2000 using production and consumption statistics. We have not extrapolated this data over the period covered by CarbonTracker-CH_4, and have instead kept prior emission estimates constant at 2000 levels. This will allow us to test whether the emission estimates suggest changes in anthropogenic emissions, for example, the large increase in emissions from coal production in Asia or the significant increase in oil and gas drilling over the last decade in North America. In some cases, the spatial distributions of priors may not be accurate since they may be based on simple assumptions like population. For other emissions, there may have been changes in the spatial distribution of emissions over the decade, oil and gas drilling in North America for example. The atmospheric inversions allow the possibility of diagnosing these problems in the underlying prior emission datasets and may lead to improvements in methodology.

2.6 Prior Emission Estimates for Agriculture and Waste

The largest source of methane emitted by human activity is agriculture and waste; emissions from rice agriculture, waste/wastewater, and animals and their waste total 230-250 Tg CH_4 yr^{-1}. Ruminants, such as cattle, goats, sheep and water buffalo are able to convert hard-to-digest forage to energy through enteric fermentation, in which microbes produce easily digested material inside the animal's gut. Emissions from enteric fermentation may be expected to increase with increasing human population and higher standards of living. Animal waste, along with wastewater and landfills produce CH_4 when conditions favor anaerobic decomposition. Organic material is decomposed in low oxygen conditions by chains of microbial processes that terminate in production of methane by methanogens.

Rice agriculture is also a significant source of methane to the atmosphere. This is because warm, waterlogged organic-rich soils in rice paddies are ideal for methanogenesis. Bottom-up estimates of emissions from rice agriculture are 50 Tg CH_4 yr^{-1}, and emissions can be significantly reduced by drainage of paddies between harvests as well as other agricultural practices (Yan et al., 2009).

CarbonTracker-CH_4 uses the 1°x1° degree gridded emissions from the EDGAR 3.2FT2000 as prior emission estimates for enteric fermentation, animal waste management, wastewater and landfills. This data set is based on emission inventories by country and sector for the years 1990 and 1995 extrapolated to 2000 using production and consumption statistics. For rice agriculture, we used the seasonally varying emissions of Matthews et al. (1991). We have not extrapolated this data over the period covered by CarbonTracker-CH_4, and have instead kept prior emission estimates constant at 2000 levels as for fossil fuel emissions.

2.7 Prior Emission Estimates for Biomass Burning

Fires are a relatively small part of the atmospheric CH_4 budget: 15-20 Tg CH_4 yr^{-1} out of a total of ~520 Tg CH_4 yr^{-1}, however, they are an important contribution to inter-annual variability of methane.

The fire prior currently used in CarbonTracker-CH_4 is based on the Global Fire Emissions Database (GFED), which uses the CASA biogeochemical model to estimate the carbon fuel in various biomass pools along with burned area based on MODIS satellite observations of fire counts (Giglio et al., 2006; van der Werf et al., 2006). The dataset consists of 1°x1° gridded monthly burned area, fuel loads, combustion completeness, and fire emissions for numerous atmospheric constituents, including CH_4 for the time period spanning January 1997 - December 2010.

2.8 Prior Estimates for Ocean Fluxes

The oceans play a relatively small role in the budget of atmospheric methane, contributing only ~2-3% of global emissions (~10-15 Tg CH_4 yr^{-1}). A significant fraction of this is assumed to come from methane seeps in shallow coastal waters (~5 Tg CH_4 yr^{-1}). The overlying water column must be shallow for emission to the atmosphere, since CH_4 is efficiently consumed by aerobic microbial processes. The water column also needs to be shallow for bubbles to deliver methane directly to the air. Coastal waters are sometimes supersaturated in CH_4, and may emit about 6 Tg CH_4 yr^{-1} to the atmosphere, while the open may add another 3 Tg CH_4 yr^{-1} (Houweling et al., 1999; Lambert and Schmidt, 1993).

Rhee et al. (2009) have suggested that global ocean emissions excluding natural seeps is much smaller than the ~9 Tg CH_4 yr^{-1} we have used in this version of CarbonTracker-CH_4, only about 0.6-1.2 Tg CH_4 yr^{-1}. On the other hand, recent studies conducted in the coastal waters of the eastern Siberian Arctic hint at the possibility of a significant source of methane coming from methane bubbling from the continental shelf sediments (Shakova et al., 2010). For this version of CarbonTracker-CH_4 we followed the approach of Bergamaschi et al. (2009) and used the estimates of Houweling et al., (1999) and Lambert and Schmidt (1993) as prior flux estimates. We also assumed an uncertainty on these prior flux estimates of ±75%.

2.9 Atmospheric Chemical Loss

Methane is removed from the atmosphere mainly by reaction with hydroxyl radical (OH), but also by reaction with atomic chlorine (Cl) and excited-state oxygen (O^1D) in the stratosphere. The chemical loss of methane over a year is about equal to the total input from sources (~520 Tg CH_4 yr^{-1}), and the mean lifetime of methane is 9-10 yr. Small differences in the emissions and losses lead to trends in atmospheric CH_4 abundance, while year to year changes in the balance of emissions and loss lead to inter-annual variability and possibly to trends in observed methane.

Hydroxyl radical is extremely reactive and has such a short atmospheric residence time that it is difficult to directly measure its global distribution. Instead, observations of atmospheric species that have relatively well-quantified anthropogenic emissions and are destroyed only by reaction with OH, such as methyl chloroform (CH_3CCl_3), are used, often along with atmospheric models, to estimate the abundance of atmospheric OH. Using an empirical approach, Montzka et al. (2011) noted that the inter-annual variability in atmospheric OH is likely to be within about ~2%. Errors in derived OH distributions arise from uncertainty in the emissions of CH_3CCl_3 used to estimate OH and uncertainties in transport models. Krol et al. (1998) estimated that the uncertainty in globally averaged OH is ±10%.

About 10% of total chemical loss is due to transport and chemical destruction in the stratosphere. A small amount of this methane-depleted air is returned to the troposphere and could influence interpretation of high-altitude (aircraft) measurements of methane. In addition, errors in simulating stratosphere-troposphere transport could result in biases for model simulations covering many years.

Errors in the chemical loss of methane and the inability to adequately resolve inter-annual variability of OH are troublesome for estimation of methane fluxes. A 2% variation in the global methane sink is equivalent to ~10 Tg CH_4 yr^{-1}, about the size of estimated inter-annual variability in methane emissions.

For the present version of CarbonTracker-CH_4 we use pre-calculated OH fields from a full-chemistry TM5 simulation that have been optimized against global observations of methyl chloroform. The chemical loss fields consist of a single, repeating seasonal cycle, and result in a methane lifetime of about 9.5 yr. Details of the chemical loss fields may be found in Bergamaschi et al. (2005).

2.10 Observational Constraints

This study uses measurements of air samples collected at surface sites in the NOAA ESRL Cooperative Global Air Sampling Network (http://www.esrl.noaa.gov/gmd/ccgg/flask.html) except those identified as having analysis or sampling problems, or those thought to be strongly influenced by local sources. The availability of data varies over time. Data collection, quality control and analysis methods are described in detail by Dlugokencky et al. (1994). A map of sites used in CarbonTracker-CH_4 is shown in Figure 1. In addition, we use in situ quasi-continuous CH_4 time series from the following towers operated by Environment Canada (EC): 30 m above ground level (agl) at Candle Lake (CDL, formerly Old Black Spruce), SK, Canada, 105m agl at East Trout Lake, SK, Canada (ETL), 40 m agl at Fraserdale, ON, Canada (FRD), and 10 m agl at Lac Labiche, AB, Canada (LLB). Other in situ quasi-continuous CH_4 time series used are from the EC Canadian sites at Alert, Nunavut (ALT), Sable Island, NS (SBL) and Egbert, ON (EGB). All observations used in CarbonTracker-CH_4 are calibrated against the WMO GAW CH_4 X2004 mole fraction scale (Dlugokencky et al., 2005).

For most quasi-continuous sampling sites, we construct an afternoon daytime average mole fraction for each day from the time series, recognizing that our atmospheric transport model does not always capture the continental nighttime stability regime while daytime well-mixed conditions are better matched. Table 1 summarizes how data from the different measurement programs are preprocessed for this study.

We further exclude non-marine boundary layer (MBL) observations that are very poorly forecasted in our framework following the strategy used with CarbonTracker-CO_2. We use the so-called model-data mismatch in this process, a quantity that represents random error ascribed to each observation to account for measurement and modeling errors at each site. If the observed-minus-forecasted mole fraction exceeds 3 times the prescribed mismatch, then the observation is not used at that time-step of the inversion. This can happen when an air sample influenced by local emissions is not captured well by our 1°x1° fluxes, or when local meteorological conditions are not captured by our offline transport fields. A complete list of sites used in CarbonTracker-CH_4 is given in Table 2, along with the model-data mismatch used, the number of points available, the number that were excluded, and statistics on the posterior fit to each site.

Model-data mismatches were determed by assigning each site to a particular category; marine boundary layer (7.5 ppb), terrestrial (30 pbb), mixed marine and terrestrial (15 or 25 ppb), tower (25 or 30 ppb) and hard to fit sites (75 ppb). The model-data mismatch values were based on evaluation of forward runs and experience gained from CarbonTracker (CO_2, Peters et al., 2005). We forced the assimilation to closely match remote marine background sites while some sites were given a very large model-data mismatch because they are likely influenced by strong local sources. A complete list of sites and their model-data mismatches is shown in Table 2.

3. Evaluation of CarbonTracker-CH_4

In this section we discuss the evaluation of CarbonTracker-CH_4 using three methods: comparison of prior and posterior residuals (difference between simulated and observed CH_4 concentration), comparisons to profiles measured from aircraft that were not used in the assimilation, and comparisons to integrated global and zonal concentration and growth rate.

3.1 Residuals

The prior and posterior residuals, calculated by subtracting the observed CH_4 mole fraction at each site constraining the inversion from the simulated prior or posterior abundances, are shown in Figure 2. The bottom panel shows that the balance between the prior emissions and the chemical sink leads to an underestimate of CH_4 relative to observations at all latitudes. By the end of the simulation, the negative bias of the model using prior fluxes reaches values up to 75 ppb (compared to a global average of ~1790 ppb in 2009, about 4%). This negative bias is considerably reduced for the posterior residuals, as is shown in the top panel, and at most sites the posterior residuals are within ~15 ppb of the observations. This is partly by design, since the model-data mismatch determines how closely the posterior CH_4 abundances must match the observations; however, as Table 1 shows, the posterior residuals even for some sites that have large model-data mismatch error assigned to them, can be quite small. An example is BKT, with a model-data mismatch of 75 ppb and a posterior residual of only 6.8 ppb. For sites like this, future inversions could use reduced model-data mismatch errors, allowing the observations to more strongly constrain the inversion.

Figure 2 shows that even after assimilation of observations, some sites have large low biases (implying emissions higher than prior estimates are needed to match the observations) and Figure 3 shows the relative sizes of the residuals. WGC (Walnut Grove, CA is located in near a densely populated urban area and agriculture and has an average posterior residual of -118 ppb. In addition to the difficulty of using relatively coarse resolution global transport to simulate observations amidst strong local sources, it is also likely that the prior emissions are underestimated. Other sites with large biases are WKT (central Texas) and SGP (Southern Great Plains, OK) with average residuals of -49 ppb and -57 ppb. These sites see transport from polluted urban areas, and they likely also see transport of emissions from oil and gas drilling as discussed in more detail below. Some of the Environment Canada sites also have large negative biases. LLB (Lac Labiche, Canada) for example, has an average residual of -80 ppb, and it is located close to possible wetland sources as well as fossil fuel operations.

3.2 Comparison to Aircraft Profiles

The current version of CarbonTracker-CH_4 does not assimilate observations from the NOAA GMD aircraft project. This network currently consists of 17 sites distributed over North America where air samples are collected at 12 altitudes and analyzed for a suite of atmospheric gases, including CH_4 (http://www.esrl.noaa.gov/gmd/ccgg/aircraft/). Because the aircraft observations were not used to constrain the inversion, these data can be used as an independent check on the inversion. In addition, they provide useful insight into the performance of TM5's vertical transport.

Figure 4 shows the prior and posterior residuals for THD (Trinidad Head, CA), where the white line represents the average of the residuals and the red lines show the standard deviation of the residuals as a function of altitude. Compared to the prior residuals, the posterior residuals show a reduction in bias at all altitudes, as well as a smaller spread in the residuals. At high altitudes the surface data constraints have resulted in estimated emissions that are in good agreement with the well-mixed free tropospheric abundances. THD shows good agreement at the lowest levels because profiles at this location are more likely to sample background marine air coming off of the Pacific Ocean. In contrast, the continental site, DND (Dahlen, North Dakota) shows a much larger negative bias at low altitudes during the summer but good agreement at all levels during winter (Figure 5). This implies that local or regional-scale sources that are not included in the CarbonTracker-CH_4 prior and are not "seen" by other sites influence these summertime profiles. Similar results are found for other aircraft sites distributed throughout the central U.S. Some sites, however, show larger biases near the surface. Figure 6 shows both prior and posterior residuals at TGC (Texas Gulf Coast), a site that sees both continental and marine air, and also air from nearby industrial and urban centers along the Texas Gulf Coast. Even after the inversion, the residuals near the surface are still quite large indicating that the priors and the observations constraining are not able to account for strong local sources.

Figure 7 shows prior and posterior residuals for Poker Flat, Alaska. Note that even after the inversion, methane abundance is underestimated near the surface. This is likely the result of underestimation of prior wetland emissions, along with observational constraints that contain information about interior Alaska. On the other hand, as we will show below Arctic sites sampling background air likely capture the large scale methane budget fairly well. Figure 7 demonstrates the importance of sampling sites near sources for constraining regional methane budgets. Future versions of CarbonTracker-CH_4 may use at least the lower levels of the aircraft observations in order to better constrain emissions.

3.3 Global and Zonal Averages

The abundance of CH_4 integrated over the global atmosphere and its growth rate are important diagnostics of inversion performance (Rayner et al., 2004; Bruhwiler et al., 2011; Bergamaschi et al., 2013) because given the ~10 year lifetime of CH_4, on global scales emissions and sinks must balance in a way that produces the observed global growth of CH_4. Here we follow the approach taken by Bruhwiler et al. (2011) that uses the same sampling, filtering and smoothing procedure used to produce the observed global and zonal CH_4 abundances for both data and model output (see Masarie and Tans (1995) and web updates at esrl.noaa.gov/gmd for a description of the data extension procedure). Zonal averages are constructed using mainly marine boundary later sites by removing a long term trend approximated as a quadratic function, deseasonalizing by subtracting an average seasonal cycle, and using a low-pass digital filter with a half width of 40 days. Importantly, the model is sampled at the same times as the observations and missing data are filled in the same way for both the observations and simulations. The simulated and observed zonal averages are therefore comparable. As shown in the top panel of Figure 8, the global posterior CH_4 abundance produced by the CarbonTracker-CH_4 assimilation is in fairly good agreement with the observed global abundance, however it is biased low by about 10 ppb. This is because the global abundance that results from use of the prior fluxes without optimization is much lower than observed, and the posterior global total represents a compromise between CH_4 abundance obtained from prior flux estimates and the observations at each site. Reducing the model-data mismatch error and/or increasing the prior flux uncertainty would improve the agreement between posterior CH_4 and the observations, but likely at the expense of having flux estimates with unrealistic spatiotemporal variability, especially in regions that are relatively unconstrained by observations. On the other hand, if the prior flux estimates are weighted too heavily in the inversion, the posterior global total more closely follows the global abundance simulated by the prior fluxes than the observations, and these may depart significantly from the actual emissions. The middle panel of Figure 8 shows the difference between the simulated and prior CH_4 abundance and the observations, where it can be seen that the residual difference varies slightly over time as the bias resulting from prior emissions changes. In particular, between 2004 and 2006, the prior residuals are fairly constant and the residual between the posterior and the observations is smaller than over other periods. The conclusions that can be drawn from this are that better prior flux estimates are needed for future versions of CarbonTracker-CH_4, and that the global abundance is a useful way to judge whether the solution is most influenced by the prior information or by the observational constraints.

The bottom panel of Figure 8 shows the growth rate of global atmospheric CH_4, a quantity that is directly related to imbalances between emissions and sinks. CarbonTracker-CH_4 follows the observed growth rate fairly well, but not perfectly since there are periods for which it under- or overestimates the observed growth rate. During 2007, for example, the observed growth was underestimated by ~30%, while during 2009 it was overestimated by about the same amount. These differences are an indication of global total biases in estimated emissions. The posterior global growth rate of CH_4 was also computed by Bergamaschi et al. (2013) for their inversions. They find a maximum growth rate of about 10 ppb yr^{-1} for 2007, closer to the observed growth rate shown in Figure 8 even when the surface observations only are used in the assimilation. This implies a possible role for the relatively short assimilation window of CarbonTracker in accounting for the underestimate in global growth. If the anomalous growth occurs in the tropics and this information cannot propagate to remote sites due to a short window, variability will be missed. As discussed by Bruhwiler et al. (2005), an assimilation window of 12 weeks is ideal for the surface network, but computational issues prevented its use for this study. On the other hand Figure 8 shows that the anomalous global growth is only slightly overestimated in 2003, while Bergamaschi et al. (2013) may underestimate this feature.

It is also informative to consider zonally averaged CH_4 mole fraction and its growth rate at sub-hemispheric scales as shown in Figure 9 for the high northern latitudes (53.1N-90N), Figure 10 for the tropics (17.5S-17.5N) and Figure 11 for the southern temperate latitudes (17.5S-53S). For the high northern latitudes, the posterior simulated integrated CH_4 is quite close to the observations and the growth rate agrees well with the observed growth rate. On the other hand, the simulated integrated CH_4 in the tropics is further from the observations and closer to the prior than for the high northern latitudes. The posterior zonal average CH_4 abundance is closer to the observations for the southern temperate latitude zone, however, the growth rate differences suggest some interannual variability differences, possibly the result of transport from tropical latitudes considering the relatively small contribution these latitudes make to the global methane budget. The simulated growth rate in the tropics also can differ significantly from the observed growth rate, with under or over estimates reaching 5 ppb/yr or more. As a comparison, the agreement between the observed and simulated growth rate at northern polar latitudes is usually well within a few ppb/yr. The middle panels of Figure 9, 10 and 11 show that when the residuals between the prior and observations decrease, the posterior residuals are also smaller.

For the high northern latitudes, a small seasonal cycle in the residuals potentially provides some information about which emission processes may be under- or overestimated by the priors. Differences between simulated and observed CH4 are largest during the winter with the observations being higher than the simulations. This implies that mid- and high latitude emissions from anthropogenic sources may be underestimated by the priors and not completely corrected for by the inversion. Note that biogenic emissions at mid- and high latitudes are at a minimum during winter.

Anomalously high growth rates were observed in 2007 both in the Arctic and in the tropics (Dlugokencky et al., 2009), a year when the Arctic was anomalously warm and the tropics were unusually wet. The results shown in Figure 9 suggest that the inversion is likely able to provide good estimates of flux anomalies in high latitudes, at least in the zonal average. For the tropics zonal average flux anomaly estimates for this year are likely to be underestimated. These differences in the ability of the inversion to recover and attribute variability are due mostly to differences in the distribution of network sites with the Arctic having better observational coverage than the tropics. Another factor is that the deep vertical mixing of the tropical atmosphere makes it difficult for the network sites that are mostly located on remote islands to detect signals from terrestrial CH_4 sources. A further limitation is the 5-week lag used in CarbonTracker's EnKF scheme that cuts off transport of signals that are transported to remote observing sites.

Note that an additional diagnostic of posterior emissions is the posterior error covariance and its difference from the prior covariance. If there are no observations to constrain the posterior estimates, then the posterior error covariance will be unchanged from the prior error covariance. While the posterior error covariance is a very useful diagnostic of the error reduction coming from observations, it is less useful as an indicator of the absolute accuracy of the estimated emissions because the accuracy of the prior estimates is ultimately not very well known, and there are transport errors that cannot be adequately accounted for.

4. Results

4.1 The High Northern Latitudes

Here the high northern latitudes are an aggregation of the Transcom 3 regions Boreal North America, Boreal Eurasia and Europe. This spatial division is somewhat awkward since some of Europe lies south of what could be considered high northern latitudes. We divide Europe into a northern section that lies poleward of 47N, and a southern section that is south of 47N, where this latitude is chosen to roughly correspond with the southern extents of Boreal North American and Boreal Eurasian source regions. The prior anthropogenic emissions suggest that ~34 Tg CH_4 yr^{-1} is emitted from northern Europe, while ~15 Tg CH_4 yr^{-1} is emitted from southern

Europe. Emissions from wetlands are much larger in the northern Europe than in the south.

The ten-year average posterior aggregated flux for the high northern latitudes is 81 ± 7 Tg CH_4 yr^{-1}, a decrease of a little over 12 Tg CH_4 yr^{-1} from the prior aggregated flux. Note that due to the use of a 5- week assimilation window, the uncertainty estimate does not include temporal error covariance over timescales longer than this period and it should therefore be regarded as the best estimate possible for the long term error covariance given the limitations of the current assimilation scheme. The inversion suggests that most of this decrease is a reduction in natural wetland emissions (8 Tg CH_4 yr^{-1}) with the remaining amount coming from fugitive fossil fuel emissions, although the portioning between these sources is strongly influenced by the prior distributions and relative locations of observation sites. Although the observing network could still be considered sparse at high northern latitudes, the number of existing sites is sufficient to reduce uncertainty by over 75% from the prior uncertainty. The total posterior flux ranges from 78 Tg CH_4 yr^{-1} in 2004 to just under 86 Tg CH_4 yr^{-1} in 2007 (Figure 12), a year that saw record warm temperatures throughout much of Boreal North America and Boreal Eurasia, as well as extremely low sea ice coverage (Stroeve et al., 2008).

Annual average methane emissions at high northern latitudes are approximately evenly divided between fugitive emissions from fossil fuels, agriculture and waste (coming mostly from Europe) and natural wetlands. As a whole, emissions from fossil fuel leakage are slightly decreased relative to prior estimates by about 4 Tg CH_4 yr^{-1} from 33 Tg CH_4 yr^{-1}, a change that is slightly larger than the posterior estimated uncertainty, 3 Tg CH_4 yr^{-1}. Note that ~ 4 Tg CH_4 yr^{-1} of the 29 Tg CH_4 yr^{-1} due to fugitive fossil fuel emissions comes from southern Europe. Emissions from agriculture and waste are unchanged. Annual average wetland emissions over the high northern latitudes are reduced by 26% from a prior of 31 Tg CH_4 yr^{-1} to about 23 Tg CH_4 yr^{-1}, a difference that is larger than the average estimated of ~ 5 Tg CH_4 yr^{-1}. This result is in agreement with previous studies (e.g. Chen and Prinn, 2006; Bergamaschi et al., 2007; Spahni et al., 2011). Our results do not agree with the emission estimates of Bloom et al. (2010). They find that only 2% of global wetland emissions come from the high northern latitudes, while we find closer to 10%. On the other hand our results agree within uncertainties with the estimates of McGuire et al. (2012) based on flux measurements. They find a source of 25 Tg CH_4 yr^{-1} from Arctic tundra wetlands with uncertainty ranging from 10.7 to 38.7 Tg CH_4 yr^{-1}. Applying the same spatial filter for their Arctic tundra region, CarbonTracker-CH_4 estimates a somewhat smaller 16 ± 5 Tg CH_4 yr^{-1}. The fact that field studies may be biased towards larger emissions could at least partially account for the lower estimate based on atmospheric observations. On the other hand, we cannot rule out the possibility that the TM5 representation of the polar atmosphere is too stable, leading to an accumulation of methane emissions in the lower atmosphere the inversion will therefore reduce emissions in order to match observations.

The estimated flux anomaly during 2007 is 4.4 ± 3.8 Tg CH_4 with a maximum summer anomaly of 2.3 Tg CH_4 in July (Figure 13). If the anomaly is calculated by subtracting the 2000-2006 average annual flux the estimated 2007 anomaly is 5.3 Tg CH_4, similar to the result found by Bousquet et al. (2011). The results of Bergamaschi et al. (2013) also seem to be consistent with these estimates (1.2-3.2 Tg CH_4). Based on zonal average analysis of network observations, Dlugokencky et al. (2009) pointed out that in 2007 the global increase of methane was equal to about a 23 Tg CH_4 imbalance between emissions and sinks, and that the largest increases in CH_4 growth occurred in the Arctic (>15 ppb/yr). This does not necessarily imply that the largest surface flux anomalies occurred at high northern latitudes. Bousquet et al. (2011) noted that the relatively weak vertical mixing characteristic of polar latitudes results in a larger response in atmospheric CH_4 mole fractions to anomalous surface emissions than at tropical latitudes where strong vertical mixing rapidly lofts surface emissions through a deep atmospheric column. Transport models therefore can play an important role in helping to untangle surface flux signals from variability in atmospheric transport processes, although care must to be taken to also consider possible biases in modeled transport.

In 2008, the flux anomalies dropped to 2.4 Tg CH_4, or 3 Tg CH_4 if the anomaly is calculated by subtracting the average annual flux over 2000-2006, as was done by Bousquet et al. (2011) who obtained 2 TgCH_4 for their INV1 that is similar to CarbonTracker-CH4, but -3 Tg CH_4 yr^{-1} using their higher spatial resolution variational inversion (INV2). As pointed out by Dlugokencky et al. (2009), both 2007 and 2008 were warm with higher than normal precipitation. Posterior covariance estimates support the independence of estimates for Boreal North America and Boreal Eurasia since the covariance between these two regions is small; however, it is difficult to accurately relate variability in observed temperature and moisture anomalies with variability in estimated emissions because of the sparseness of the surface observation sites.

For the high northern latitudes CarbonTracker-CH_4 is able to distinguish between different CH_4 source processes and regions. Wetlands may be distinguished from anthropogenic sources because of the spatial separation of prior flux constraints; many high northern latitude wetland complexes are located in relatively sparsely populated areas, while fossil fuel and agricultural and waste emissions are distributed mainly in populated areas of Europe (although the Western Siberian Lowlands is also a region of intensive fossil fuel production). Ocean methane fluxes are thought to be small compared to terrestrial fluxes, and northern Eurasia and boreal North America are separated by the North Pacific Ocean. Furthermore, the stronger zonal and weaker vertical transport characteristic of the high latitudes helps to transport flux information to network sites. Both Europe and boreal North America are at least partially constrained by surface network sites, and although boreal Eurasia is not adequately covered by network sites, a number of sites exist downwind of it (Shemya, Barrow and Cold Bay). For Europe, average trajectory calculations suggest that a large region of wetlands in eastern Scandinavia and northwestern Russia is constrained by Pallas, Finland. Other sites help to constrain the anthropogenic sources from the rest of Europe.

For boreal North America, prior flux emissions from fossil fuels and agriculture and waste form an insignificant part of total methane emissions. This is not the case for Europe for which emissions are more evenly divided between anthropogenic and wetland emissions. Note that about 40% of the agricultural emissions and 22% of the fossil fuel emissions are from southern Europe. Prior emission estimates from natural sources for Europe, the majority of which lie in northern Europe, are about 45 Tg CH_4 yr^{-1} during the summer months while the 11-year average posterior summer estimate is about 13 Tg CH_4 yr^{-1}, a large reduction. The uncertainty estimates, however, only decrease by at most 15% implying that the sources categories are not strongly constrained by observatios. Boreal Eurasian summertime wetland emissions are increased relative to the prior flux estimates from 26 Tg CH_4 yr^{-1} to 37 Tg CH_4 yr^{-1}, and posterior uncertainties decrease from prior uncertainties by ~20-25%. For boreal North America, the average posterior summer wetland flux is only slightly below the prior flux estimate (about 19 Tg CH_4 yr^{-1} compared to about 16 Tg CH_4 yr^{-1}, a difference that is within the summer average posterior estimated uncertainty of ~10 Tg CH_4 yr^{-1}). The redistribution of emissions from Europe to northern Eurasia was found by Chen and Prinn (2006) to be sensitive to the choice of sites used in the inversion, however, our results indicate that the observations imply that while prior emissions are too high for Europe, larger emissions are still needed elsewhere to match the meridional distribution of observed methane. Bergamaschi et al. (2005) also found decreased emissions for Europe relative to prior estimates, but interestingly, their inversion also reduced high-latitude emissions from prior estimates for other high latitude source regions as well. During the winter months, when biogenic emissions are low, prior estimates are decreased by the inversion for both Boreal Eurasia (-20%) and Europe (-8%) and relatively unchanged for boreal North America. The small change in winter European emissions supports the conclusion that prior wetland emissions for Europe are indeed overestimated. Note that prior emissions for wetland emissions from northern Europe are about equal to fugitive emissions from fossil fuels.

High latitude emissions of CH_4 from agriculture and waste are significant only for Europe, and estimated fluxes are unchanged from prior estimates. Fugitive emissions of CH_4 from fossil fuel production are reduced from prior estimates for Europe and boreal Eurasia by 2 Tg CH_4 yr^{-1} for each region; from 21 ± 4 Tg CH_4 yr^{-1} and 12 ± 2 Tg CH_4 yr^{-1}. Reductions in uncertainty are fairly large for Europe, ~35%, and about ~32% for Boreal Eurasia. For boreal North America, prior estimates of fossil fuel emissions of CH_4 are very small (< 1 Tg CH_4 yr^{-1}), and it should be noted that the tar sand production areas are in the temperate North American TransCom 3 source region rather than Boreal North America.

Significant natural CH_4 emissions have recently been proposed for the high northern latitudes. Walter et al., (2007) estimated that in addition to emissions from High Northern Latitude wetlands (31 Tg CH_4 yr^{-1} for the CarbonTracker-CH_4 prior), ebullition from arctic lakes could add an additional 24 ± 10 Tg CH_4 yr^{-1}. In addition to organic rich sediments and subsea permafrost, CH_4 is stored in ice hydrates forming at the low temperatures and high pressures in sediments at the bottom of the Arctic Ocean and subsea permafrost, and below terrestrial permafrost as well. Relatively shallow waters make it possible for bubbles to transport methane directly and rapidly to the atmosphere. The estimates of Shakhova et al. (2013) estimate the size of the source from subsea permafrost from the East Siberian shelf alone to be ~17 Tg CH_4 yr^{-1}, although observational records are currently insufficient to establish whether these emissions are changing over time. Walter et al. (2012) have proposed that a similar process may also occur on land as permafrost thaws and glaciers melt. Total natural emissions including all of these processes approaches 65 Tg CH_4 yr^{-1}, an amount that significantly exceeds both the average prior and posterior annual natural emissions for CarbonTracker-CH_4 (31 and 23 Tg CH_4 yr^{-1}). Since the average total posterior CarbonTracker-CH_4 high northern latitude emissions is ~81 Tg CH_4 yr^{-1}, accommodation of a 65 Tg CH_4 yr^{-1} natural source would have to come at the expense of fossil fuel and agriculture/waste sources (average total CarbonTracker-CH_4 posterior of ~57 Tg CH_4 yr^{-1}, with about 12 Tg CH_4 yr^{-1} emitted from southern Europe), which would need to be reduced by about 75%.

The estimated mass of carbon thought to be frozen in Arctic permafrost down to 20 m is estimated to be ~1700 Pg C (Pg = 10^{15} g) (Tarnocai et al., 2009), significantly more carbon than is currently in the atmosphere (~830 Pg C) and over 3 times what has already been emitted to the atmosphere from fossil fuel use since pre-industrial times. As the Arctic warms and permafrost thaws, this ancient carbon may be mobilized to the atmosphere and a small fraction (~3%) may be emitted as CH_4 (Schuur et al., 2011). Recent studies suggest that permafrost carbon will begin to enter the atmosphere during this century (e.g. Schaefer et al., 2010; Harden et al., 2012; Melton et al., 2013; Frolking et al., 2011). Harden et al. (2012) predict that 215-380 PgC will thaw by 2100. Their assessment of the carbon balance of Arctic tundra based on flux observations McGuire et al. (2012) found that between the 1990s and 2000s emissions of CH_4 doubled (from 13 to 26 Tg CH_4 yr^{-1}), results that are consistent with warmer temperature and longer growing seasons.

Detection of trends in Arctic greenhouse gas emissions is difficult using atmospheric concentration measurements alone because changes are expected to be small in comparison to transport of much larger mid-latitude emissions. Forward and inverse modeling techniques can be helpful because they provide the ability to untangle variability coming from transport from signals associated with local sources. As shown in Figure 13, posterior CarbonTracker-CH_4 emissions do not indicate that there has been a trend in natural high northern latitude emissions over the last decade, although we see strong evidence for substantial inter-annual variability.

4.2 The Northern Hemisphere Mid-Latitudes

For this study, the northern mid-latitudes are composed of the temperate Eurasia and temperate North America Transcom 3 regions (see Figure 1). The average estimated total emissions for the northern mid-latitudes over the period 2000-2010 are greater than prior estimates by about 5 Tg CH_4 yr^{-1}, increasing from about 156 ± 27 Tg CH_4 yr^{-1} to 162 ± 16 Tg CH_4 yr^{-1}. After the tropics, the Northern Hemisphere mid-latitudes emit the most atmospheric CH_4. The largest mid-latitude source of CH_4 is agriculture and waste, and this source rises from 117 ± 26 Tg CH_4 yr^{-1} to 119 ± 15 Tg CH_4 yr^{-1}. Natural wetlands are a fairly small contribution to northern mid-latitude emissions, and they are increased from about 9 ± 3 to 12 ± 2 Tg CH_4 yr^{-1}. For the northern mid-latitudes as a whole, estimated fossil fuel emissions remain very close to prior estimates at about 31 ± 3 TgCH_4.

In general, CarbonTracker-CH_4 re-distributes prior estimated emissions from temperate Eurasia to North America (Figure 14). The total prior flux estimates for temperate Eurasia and temperate North America are 124 ± 22 and 32 ± 5 Tg CH_4 yr^{-1}, respectively. The average posterior estimates are 114 ± 15 and 47 ± 3 Tg CH_4 yr^{-1}. Agriculture and waste emissions from temperate Eurasia are reduced by almost 10 Tg CH_4 yr^{-1} (~9%). Fugitive fossil fuel emissions for temperate North America increase by ~9% (6.7 ± 1.5 to 8 ± 1 Tg CH_4 yr^{-1}), agriculture and waste emission increase by 53% (21 ± 4 to 32 ± 3 Tg CH_4 yr^{-1}), and natural emissions increase by 66% (4.5 ± 1 Tg CH_4 yr^{-1} to 7.5 ± 1 Tg CH_4 yr^{-1}). Posterior uncertainties for both regions decrease from prior uncertainty by about 30%.

In this version of CarbonTracker-CH_4, we used constant anthropogenic emissions representative of the year 2000 from the EDGAR v3.2 FT database as priors. A more recent version of EDGAR (version 4.2, (European Commission, JRC, 2009) reports that global anthropogenic emissions of methane significantly increased over the last decade, from 309 Tg CH_4 yr^{-1} in 2000 to 364 Tg CH_4 yr^{-1} by 2008 (an increase of about 18%). Most of this increase (37 Tg CH_4 yr^{-1}) is estimated to have occurred between 2000 and 2006 according to EDGAR. As we show in Figure 8, the observed global total CH_4 does not change much between 2000 and 2005. Bousquet et al. (2006) proposed that increased anthropogenic emissions were balanced by decreases in wetland emissions for the early 2000s CarbonTracker-CH_4 is constrained using a time-invariant prior, and because it must follow the observed global growth rate that flat at least until 2006, it does not find trends in either total anthropogenic or natural emissions.

After 2006 the observed global annual mean CH_4 abundance increased ~25 ppb by 2010, equivalent to additional emissions of ~70 TgCH_4 over 4 years (18 Tg CH_4 yr^{-1}) if mixed uniformly throughout the atmosphere. As discussed in section 3.3, CarbonTracker-CH_4 follows the global growth rate closely. The average total emissions from 2000 to 2006 are ~514 ± 22 TgCH_4, but after 2006 it is 530 ± 22 Tg CH_4 yr^{-1}, an amount that is in approximate agreement with the change in total emissions implied by observations. CarbonTracker-CH_4 allocates much of this increase to anthropogenic sources. Average global total anthropogenic emissions are 316 ± 18 Tg CH_4 yr^{-1} for 2000 to 2005, increasing to 325 ± 18 Tg CH_4 yr^{-1} for 2006 to 2010, a number that is roughly consistent with the constant anthropogenic prior inversions of Bergamaschi et al. (2013). For the period 2000 to 2005, the estimated total natural emissions are 198 ± 12 Tg CH_4 yr^{-1}, increasing to 204 ± 12 Tg CH_4 yr^{-1} from 2006 to 2010. CarbonTracker-CH_4 assigns the post-2005 estimated increases in anthropogenic emissions to the populated northern temperate latitudes, while the bulk of the global increase in natural emissions is assigned to the tropics.

The EDGAR emission data imply that anthropogenic emissions of CH_4 grew rapidly over the last decade, with significant growth occurring between 2000 and 2005, a time when the observed growth rate does not support an upward trend in emissions. Could decreased emissions from wetlands have cancelled out this increase as Bousquet *et al.* proposed? More recent work by Bergamaschi et al. (2013) suggests a large role for anthropogenic emissions, while Houweling et al. (2013) find that a mixture of anthropogenic and tropical wetland sources are responsible for the increase since 2006. Although the sparseness of the observational network makes it impossible to rule this scenario out, the observations and the spatial constraint they supply to the inversion do not suggest that there was a trend in wetland emissions over the first half of the decade, although there certainly was inter-annual variability. On the other hand, this result cannot be reconciled with bottom-up estimates of increasing anthropogenic emissions over this period. From 2006 through 2010, estimated emissions increased by ~15 Tg CH_4 yr^{-1}, slightly less than the 18 Tg CH_4 yr^{-1} estimated by EDGAR for this period, and with considerable inter-annual variability. CarbonTracker-CH_4 divides this growth between anthropogenic and natural emissions in proportion to their contribution to the prior global atmospheric CH_4 budget (~60% anthropogenic and ~40% natural). Although it is likely that both anthropogenic and natural emissions have been increasing since 2006, this latter fact may also be interpreted as evidence of the inability of the observational network to discriminate between these categories of sources due to insufficient spatial coverage at lower latitudes. It is possible that the use of observed isotopic composition of CH_4 could help to distinguish different sources (e.g. Miller et al., 2002). Uncertainty reductions are substantial for the global totals of both natural and anthropogenic emissions, ~66% each, and this suggests that observational constraints are consistent with the prior allocation of emissions between natural and anthropogenic processes, but does not rule out the possibility that the network cannot discriminate between the two. Bergamaschi et al. (2013) have also suggested that the increases in anthropogenic emissions from EDGAR are likely too high, especially estimates of emissions from Chinese coal production.

Anthropogenic emissions from Asia are thought to have been increasing steeply in recent years. EDGAR v4.2 emissions dataset estimates that total anthropogenic emissions from China increased from about 50 Tg CH_4 yr^{-1} in 2000 to over 73 Tg CH_4 yr^{-1} in 2008, an increase of almost 50%. CarbonTracker-CH_4 does not show a steady upward trend in emissions from temperate Asia, but there is a 5 Tg CH_4 yr^{-1} increase between the average of the first and last five years, a change that is well within the estimated uncertainty for this region of 15 Tg CH_4 yr^{-1}. This is consistent with the ~5 Tg CH_4 yr^{-1} increase in anthropogenic emissions from China between 2003 and 2008 found by Bergmaschi et al. (2013). For temperate North America, there does not appear to be much change over the decade in total estimated emissions; however, fugitive emissions from fossil fuel production in temperate North America show significant increases from prior emissions during winter months, when biogenic emissions are smallest (Figure 15). By the end of the decade, winter fossil fuel emissions from temperate North America end up higher than prior flux estimates by about 4 Tg CH_4 yr^{-1}, exceeding the estimated uncertainty of ~3 Tg CH_4 yr^{-1}. Due to large variability of biogenic emissions, it is difficult to see evidence of this change during the warmer seasons, and the variability also may mask evidence of increasing fossil fuel emissions in the total estimated emissions. It is interesting to note that, as shown in Table 1, many of the sites with the largest residuals are located near potential sources of fugitive emissions from fossil fuel use. An example is SGP (Southern Great Plains) located in northern Oklahoma. Figure 16 shows that it is increasingly difficult over time for the inversion to fit this site, possibly due to increasing emissions from fossil fuel production nearby and in northern Texas. This feature is qualitatively consistent with the results of Miller *et al.* (2013), who calculated larger than predicted emissions of CH_4 related to fossil fuel extraction in this part of the USA, although they also acknowledge a possible role for emissions from livestock. The recent expansion of oil and gas production is not included in the prior used for CarbonTracker-CH_4, and the more recent EDGAR4.2 emission product has more emissions in North America than the prior we used here. Petron et al. (2012) have recently suggested that leakage from fossil fuel production in Colorado's Denver-Julesburg Basin may be several times larger that estimated by state and local inventories. Karion et al. (2013) have recently shown that emissions from a gas field in Utah may be much higher that previous estimates as well.

4.3 The Tropics

Tropical emissions are difficult to constrain because of the sparse distribution of atmospheric observations, but also due to the tendency of the tropical atmosphere to rapidly mix surface signals throughout a deep atmospheric column. Many of the observation sites in tropical latitudes are located on islands where they sample marine air from higher latitudes. Ascension Island, for example often sees air from the South Atlantic, rather than air transported westward from tropical Africa. Although the site located in the Seychelles site sometimes sees air from southern Asia, often it sees air transported from the southern Indian Ocean. In particular, it is difficult to see how the current observational network can independently constrain tropical Asia and tropical Africa. On the other hand, Pacific Ocean sites may make it possible to discriminate between tropical America and Asia.

In agreement with the results found by other studies (e.g. Houweling et al., 1999; Bergamaschi et al., 2007; Mikaloff–Fletcher et al., 2004a,b, Houweling et al., 2013), CarbonTracker-CH_4 increases tropical emissions relative to prior estimates. The average total prior emission is 132 ± 18 Tg CH_4 yr^{-1} and the posterior total is about 157 ± 11 Tg CH_4 yr^{-1}, an increase of 19%. The estimated uncertainty is ±11 Tg CH_4 yr^{-1}, a decrease from the prior uncertainty of about 39%. This suggests that the observations are able to add some information about tropical emissions to the inversion. Most of the adjustment in emissions goes to wetlands (an increase of 31% from ~65 Tg CH_4 yr^{-1} to ~84 Tg CH_4 yr^{-1}, with a decrease in uncertainty from 14 to 8 Tg CH_4 yr^{-1}, or 57%). Posterior anthropogenic emissions are essentially unchanged from priors with posterior emissions of 49 Tg CH_4 yr^{-1} for agriculture and waste, and ~7.5 Tg CH_4 yr^{-1} for fossil fuel emissions, with the uncertainty in total anthropogenic emissions decreasing from 11 Tg CH_4 yr^{-1} to about 7 Tg CH_4 yr^{-1}. CASA-GFED prior flux estimates for biomass burning are increased from about 10 Tg CH_4 yr^{-1} to 11 Tg CH_4 yr^{-1}.

Interestingly, the estimated increases in decadal-average emission from tropical wetlands are not evenly distributed among the tropical regions of South America, Africa and Asia. Changes are largest for South America, increasing from a prior of about 19 ± 4 Tg CH_4 yr^{-1} to almost 32 ± 4 Tg CH_4 yr^{-1} (+68%). For Africa, posterior emissions increase from 17 ± 4 Tg CH_4 yr^{-1} to 21 ± 4 Tg CH_4 yr^{-1} (+24%) and for Asia, 29 ± 6 Tg CH_4 yr^{-1} to 35 ± 6 Tg CH_4 yr^{-1} (+21%). The estimates from CarbonTracker-CH_4 compare well with Melack et al. (2004), who estimate that the Amazon basin emits about 29 Tg CH_4 yr^{-1} using a combination of field studies and satellite observations of wetland extent. Estimated emissions from anthropogenic sources remain very close to prior estimates for all tropical regions, and this is also the case for biomass burning. For all tropical regions, the posterior uncertainty is only slightly reduced with respect to the prior uncertainty, generally less than 15%, and the high posterior correlations between these regions make it difficult to have confidence that the inversion is able to constrain information about these regions.

Although observations indicate inter-annual variability in the CH_4 growth rate in the tropical marine boundary layer, CarbonTracker-CH_4 is not able to capture this very well as discussed in the previous section on evaluation. Figure 17 shows both the increase in posterior CH_4 emission estimates from the prior, as well the inter-annual variability of the estimates. Total biogenic emissions (e.g. agriculture/waste and wetlands) were larger than normal during 2007 and 2008 in agreement with the analysis of Dlugokencky et al. (2009), who noted that both of these years were relatively wet in the tropics. Wet years are also years with lower fire emissions and the posterior emissions of CarbonTracker-CH_4 show a significant anti-correlation of fire and wetland emissions as shown in Figure 18, although the estimated uncertainties on the emission anomlies are quite large.

Increases in tropical emissions for 2007 and 2008 are also found by Bergamaschi et al. (2013) although they show interesting differences between their inversions that used space-based observations and those using only surface observations. Houweling et al. (2013) showed that use of space-based observations with a bias correction that is fixed using independent data rather than estimated by the inversion results in a re-distribution of emissions from the extra-tropical Northern Hemisphere to the tropics by ~50 Tg CH_4 yr^{-1}. Their tropical emissions over 2003 to 2010 range from 380 to 450 Tg CH_4 yr^{-1}, much higher than the values obtained by this study, although the latitude range of their tropics is not clear. CarbonTracker-CH_4 values are similar to Houweling et al. (2013) if we use 30S-30N as the latitude range of the tropics. In addition, Houweling et al. (2013) note that they estimate larger inter-annual variability in tropical emissions of CH_4 using their preferred bias correction methodology. Although this may indicate that the space-based observations are adding significant new information to the inversion, as noted by Houweling et al. (2013), degradation of the instrument occured after 2005.

In addition to a greatly needed expansion of sites sensitive to the tropical biosphere [e.g. Miller *et al.*, 2007], progress on constraining tropical emissions could be made by increasing the length of the assimilation window, allowing signals to reach existing observation sites from terrestrial tropical source regions, and by using aircraft observations as constraints in the assimilation. Also since CarbonTracker-CH_4 seems to miss tropical variability in emissions, it is likely that the growth in global CH_4 abundance due to tropical wetlands is be greater than the posterior estimates suggest. Comparisons of posterior CH4 profiles with profiles measured aircraft at two sites in Brazil (Fortaleza on the coast, and Santarem in the interior) support both the underestimate of emissions in the priors and the lack of data to revise the priors adequately. This was pointed out aslo by Beck et al. (2012).

Since setting up and maintaining observation sites in tropical land regions is logistically difficult, coverage may never be adequate in these regions. The hope is that remote sensing observations could provide additional observational constraints, however, the issue of how to identify and quantify biases in remotely sensed CH_4 that are be spatially and temporally coherent is still be an important limitation (Houweling et al., 2013).

4.4 The Southern Hemisphere Mid-Latitudes

Decadal mean CH_4 emission estimates from southern temperate latitudes (Temperate South America, South Africa and Australia) increase from a prior of 78 Tg CH_4 yr^{-1} to 91 Tg CH_4 yr^{-1}, an increase of about 17%. The aggregated uncertainty estimate decreases from about 12 Tg CH_4 yr^{-1} to 7 Tg CH_4 yr^{-1}, a decrease of about 40%. The largest estimated CH_4 emissions are from temperate South America (54 ± 6 Tg CH_4 yr^{-1}), followed by temperate South Africa (22 ± 2 Tg CH_4 yr^{-1}) and Australia/New Zealand (15 ± 2 Tg CH_4 yr^{-1}). Annual average flux estimates for the aggregated total emissions, as well as the individual processes are little changed from prior estimates for both temperate southern Africa and Australia/New Zealand. The posterior uncertainty estimates for these regions are essentially unchanged as well, indicating a lack of significant observational constraints for these regions.

On the other hand, aggregated total emissions for temperate South America are adjusted from 43 ± 7 Tg CH_4 yr^{-1} to 54 ± 6 Tg CH_4 yr^{-1}, although with a relatively small uncertainty reduction of about 9%. The adjustment to CH_4 emissions occurs as an increase from natural biogenic sources, since fossil fuel emissions and agriculture/waste prior flux estimates are small for this region. Emissions from natural wetlands increase by 7 Tg CH_4 yr^{-1} over prior estimates, and agriculture and waste by close to 4 Tg CH_4 yr^{-1}. The uncertainty reduction for natural wetlands is very small, while uncertainty estimates for agriculture and waste are about 13% smaller than the priors.

4.5 The Global Ocean

Emissions of CH_4 from oceans are thought to make only a small contribution to the atmospheric CH_4 budget, with a prior flux estimate in CarbonTracker-CH_4 of ~15 ± 13Tg CH_4 yr^{-1}. Posterior estimates are adjusted downwards to 12.6 Tg CH_4 yr^{-1}, a difference that exceeds the posterior uncertainty estimate of about 15 Tg CH_4 yr^{-1}. Rhee et al. (2009) have proposed that earlier estimates of the oceanic methane emissions were biased towards supersaturated waters, and that the emissions are much lower, about 0.6-1.2 Tg CH_4 yr^{-1}, a decrease of over a factor of 10. It is therefore possible that future versions of CarbonTracker-CH_4 will not include estimation of ocean emissions. Note that the ocean source does not include ebullition from methane seeps and subsea permafrost (e.g. Shakhova et al., 2010). The size and variability of emissions from this source are not currently well understood, but since significant flux to the atmosphere can only occur in relatively shallow waters, this source would likely be aliased with terrestrial sources by CarbonTracker-CH_4.

5. Conclusions

We have created an assimilation system for atmospheric methane, CarbonTracker-CH_4 and used it to estimates CH_4 emissions during 2000-2010 over large spatial scales. We find that simulated CH_4 mole fractions calculated using optimized emissions at each measurement site agree well with observations with an average bias of -10.4 ppb. Also, comparison of posterior methane profiles with measurements of CH_4 vertical profiles from aircraft that were not used in the assimilation show very good agreement, giving further confidence in the estimated emissions over large scales, as well as the representation of the transport processes that maintain the free-tropospheric CH_4 abundances. Large underestimates of CH_4 abundance can sometimes occur at the lower levels of the aircraft profiles in regions where there are likely strong local/regional sources that cannot be resolved by the spatial resolution of the system, are underestimated by the prior emission estimates, and/or not "seen" by other sites. This implies that use of aircraft data could supply important constraints for future inversions.

We have also demonstrated the diagnostic value of globally and zonally integrated CH_4 abundances. Comparison of observed and estimated global CH_4 abundances allows determination of the relative importance of prior estimates and observational constraints to the solution. Likewise, comparison of observed and posterior CH_4 mole fractions integrated over latitude zones indicates whether observational constraints are sufficient to capture observed temporal variability. Since the growth rate of globally and zonally integrated CH_4 abundance directly reflects changes in emissions and sinks, comparison of observed and simulated integrated growth provides insight into whether the inter-annual variability of fluxes is accurately recovered. Indeed we have shown that CarbonTracker-CH_4 is able to simulate the observed zonal average mole fractions and capture inter-annual variability in emissions quite well at high northern latitudes. In contrast, CarbonTracker-CH_4 is less successful in the tropics where it misses significant variability and is more influenced by prior flux estimates. This is expected given the limited number of tropical network sites and the short smoother EnKF time window.

CarbonTracker-CH_4 posterior estimates of total fluxes at high northern latitudes are about 81 ± 7 Tg CH_4 yr^{-1}, about 12 Tg CH_4 yr^{-1} (13%) lower than prior estimates, a result that is consistent with other atmospheric inversions. Emissions from European wetlands are decreased by 30%, as found by Bergmaschi et al. (2005); however, unlike their results, emissions from wetlands in Boreal Eurasia are increased. Although CarbonTracker-CH_4 does not estimate increases in emissions from high northern latitudes over the decade covered by the inversion, significant inter-annual variability is recovered. During the exceptionally warm and wet summer of 2007, estimated emissions were higher than the decadal average by 4.4 ± 3.8 Tg CH_4. It is encouraging that CarbonTracker-CH_4 estimates for the Arctic agree reasonably well and within estimated uncertainties with the analysis of flux observations by McGuire et al. (2012), although they are somewhat lower (16 ± 5 Tg CH_4 yr^{-1} compared to 25 Tg CH_4 yr^{-1}).

CarbonTracker-CH_4 estimates for temperate latitudes are slightly increased over prior estimates, but about 10 Tg CH_4 yr^{-1} is redistributed from Asia to North America, an amount that exceeds the posterior uncertainty estimate for North America (± 3.5 Tg CH_4 yr^{-1}). We used time invariant prior flux estimates for 2000 through 2005 when the growth rate of global atmospheric CH_4 was relatively small, so the assimilation does not estimate changes in natural or anthropogenic emissions. After 2006, when atmospheric CH_4 began to increase again, CarbonTracker-CH_4 allocates some of the emission increases to anthropogenic emissions at temperate latitudes, and some to tropical wetland emissions. The impact of increases in anthropogenic emissions from Asia implied by bottom up production statistics are not seen in the posterior flux estimates, but for temperate North America, the prior flux estimates are increased by about 4 Tg CH_4 yr^{-1} during winter when signals from much larger biogenic emissions are small, and amount that is larger than the estimated uncertainty of 3 Tg CH_4 yr^{-1}. Examination of the residuals at North American observation sites suggests that increased CH_4 emissions from gas and oil exploration may play a role.

The tropics are not currently well resolved by CarbonTracker-CH_4 due to sparse observational coverage and a short smoother window. However, posterior uncertainties are slightly reduced from prior uncertainties and posterior emissions are about 18% higher than prior estimates. Most of this increase is allocated to tropical South America rather than being distributed over all tropical regions. Our estimates for tropical South America are about 32 ± 4 Tg CH_4 yr^{-1}, in good agreement with the analysis of Melack et al. (2004), who obtained 29 Tg CH_4 yr^{-1} for the Amazon Basin.

As we have shown using CarbonTracker-CH_4, even with the current sparse observational network it is possible to be able to draw conclusions about continental budgets of atmospheric CH_4 and to track and attribute variability in relatively well-sampled regions. However, information about fluxes at policy relevant scales remains elusive without increased observational coverage. This is especially true in the tropics, where droughts and flooding may have significant impact on emissions.

Acknowledgements

This work, including the measurements that formed the basis for the study, were funded in part by NOAA's Atmospheric Chemistry, Carbon Cycle and Climate Program. The authors would like to thank Martin Krol, Wouter Peters, Sander Houweling, Peter Bergamaschi and members of the TM5 Modeling Group for their support and helpful suggestions. The authors would also like to thank Elton Chan for his helpful comments, and two anonymous reviewers for their suggestions.

References

Bartlett, K. B. and R.C. Harriss, (1993), Review and assessment of methane emissions from wetlands, Chemosphere, 26, 1-4, 261-320, http://dx.doi.org/10.1016/0045-6535(93)90427-7.

Beck, V., H. Chen, C. Gerbig, P. Bergamaschi, L. Bruhwiler, S. Houweling, T. Roeckmann, O. Kolle, J. Steinbach, T. Koch, C.J. Sapart, C. van der Veen, C. Frankenberg, M. O. Andreae, P. Artaxo, K.M. Longo, S.C. Wofsy, (2012), Methane airborne measurements and comparison to global models during BARCA, *J. Geophys. Res. 117*, D15310, doi:10.1029/2011JD017345.

Bekryaev, R., I.V. Polyakov, and V. A. Alexeev, (2010) Role of polar amplification in long-term surface air temperature variations and modern Arctic warming, *J. Climate, 23*, pp. 3888-3906, doi:10.1175/2010JCL13297.1.

Bergamaschi, P., S. Houweling, A. Segers, M. Krol, C. Frankenburg, R. A. Scheepmaker, E. Dlugokencky, S. C. Wofsy, E. A. Kort, C. Sweeney, T. Schuck, C. Brenninkmeijer, H. Chen, V. Beck, C. Gerbig, (2013), Atmospheric CH_4 in the first decade of the 21st century: Inverse modeling analysis using SCIAMACHY satellite retrievals and NOAA surface measurements, *J. Geophys. Res., 118*, 7350-7369, doi:10.1002/jgrd.50480.

Bergamaschi, P., C. Frankenberg, J. F. Meirink, M. Krol, M. G. Villani, S. Houweling, F. Dentener, E. J. Dlugokencky, J. B., L. V. Gatti, A. Engel, I. Levin, (2009), Inverse modeling of global and regional CH_4 emissions using SCIAMACHY satellite retrievals, *J. Geophys. Res., 114*, D22, DOI: 10.1029/2009JD012287.

Bergamaschi, P., C. Frankenberg, J.F. Meirink, M. Krol, F. Dentener, T. Wagner, U. Platt, J. O. Kaplan, S. Korner, M. Heimann, E.J. Dlugokencky, and A. Goede (2007) Satellite chartography of atmospheric methane from SCIAMACHY on board ENVISAT: 2. Evaluation based on inverse model simulations, *J. Geophys. Res.*, *vol. 112*, doi:10.1029/2006JD007268.

Bergamaschi, P., M. Krol, F. Dentener, A. Vermeulen, F. Meinhardt, R. Graul, M. Ramonet, W. Peters and E.J. Dlugokencky, (2005) Inverse modeling of national and European CH4 emissions using the atmospheric zoom model TM5, *Atmos. Chem. Phys., 5*, 2431-2460, www.atmos-chem-phys.org/acp/5/2431.

Bloom, A.A., P. Palmer, A. Fraser, D. Reay, and Christian Frankenberg, (2010) Large-scale controls of methanogenesis inferred from methane and gravity spaceborne data, *Science, 327*, 322-325. doi: 10.1126/science.1175176.

Bousquet, P., B. Ringeval, I.Pison, E.J. Dlugokencky, E. -G. Brunke, C. Carouge, F. Chevallier, A. Fortems-Cheiney, C. Frankenberg, D.A. Hauglustaine, P.B. Krummel, R.L. Langenfelds, M. Ramonet, M. Schmidt, L.P. Steele, S. Szopa, C. Yver, N. Viovy, and P. Ciais, (2011) Source attribution of the changes in atmospheric methane for 2006-2008, *Atmos. Chem. Phys., 11*, 3689-3700, www.atmos-chem-phys.net/11/3689/2011, doi:10.5194/acp-11-3689-2011.

Bruhwiler L.M.P., A.M. Michalak and P. Tans, Spatial and temporal resolution of carbon flux estimates for 1983–2002, *Biogeosciences, 8*, 1309-1331, doi:10.5194/bg-8-1309-2011, 2011.

Bruhwiler L., A.M. Michalak, W. Peters, D. Baker, and P. Tans, An improved Kalman smoother for atmospheric inversions, *Atmos. Chem Phys., 5,*1-12, 2005.

Chen, Y.-H. and Prinn, R.G., (2006) Estimation of atmospheric methane emissions between 1996 and 2001 using a three-dimensional global chemical transport model, J. Geophys. Res., 111, D10307, doi:10.1029/2005JD006058.

Denman, K. L., Brasseur, G., Chidthaisong, A., Ciais, P., Cox, P. M., Dickinson, R. E., Hauglustaine, D., Heinze, C., Holland, E., Jacob, D., Lohmann, U., Ramachandran, S., da Silva Dias, P. L., Wofsy, S. C., and Zhang, X.: Couplings Between Changes in the Climate System and Biogeochemistry, in: Climate Change 2007: The Physical Science Basis. Contribution of Working Group I to the Fourth Assessment Report of the Intergovernmental Panel on Climate Change, edited by: Solomon, S., Qin, D., Manning, M., Chen, Z., Marquis, M., Averyt, K. B., Tignor, M., and Miller, H. L., Cambridge University Press, Cambridge, UK and New York, NY, USA, 2007.

Dlugokencky, E. J., R. C. Myers, P. M. Lang, K. A. Masarie, A. M. Crotwell, K. W. Thoning, B. D. Hall, J. W. Elkins and L. P. Steele, (2005), Conversion of NOAA atmospheric dry air CH4 mole fractions to a gravimetrically prepared standard scale, *JGR-Atmospheres*, 110, D18, doi:10.1029/2005JD006035.

Dlugokencky, E. J., L. Bruhwiler, J. White, L. Emmons, P. Novellie, S. Montka, K. Masarie, P. Lang, A. Crotwell, J. Miller, and L. Gatti (2009), Observational constraints on recent increases in the atmospheric CH_4 burden, *Geophys. Res. Lett.*, 36, L18803, doi:10.1029/2009GL039780.

Dlugokencky, E.J., Houweling, S., Bruhwiler, L., Masarie, K.A., Lang, P.M., Miller, J.B. and Tans, P.P. (2003), Atmospheric methane levels off: Temporary pause or a new steady-state? Geophysical Research Letters **30**: 10.1029/2003GL018126.

Dlugokencky, E. J., L. P. Steele, P. M. Lang and K. A. Masarie, (1994), The growth rate and distribution of atmospheric methane, *Journal of Geophysical Research*, 99, D8, 17, doi:10.1029/94JD01245.

Etheridge, D. M., L. P. Steele, R. J. Francey, and R. L. Langenfelds (1998), Atmospheric methane between 1000 A.D. and present: Evidence of anthropogenic emissions and climatic variability, J. Geophys. Res.,103(D13), 15,979–15,993, doi:10.1029/98JD00923.

European Commission, Joint Research Centre (JRC)/Netherlands Environmental Assessment Agency (PBL). Emission Database for Global Atmospheric Research (EDGAR), release version 4.0. http://edgar.jrc.ec.europa.eu, 2009.

Forster, P., Ramaswamy, V., Artaxo, P., Berntsen, T., Betts, R., Fahey, D. W., Haywood, J., Lean, J., Lowe, D. C., Myhre, G., Nganga, J., Prinn, R., and Raga, G., M. S. a. R. V. D.: Changes in Atmospheric Constituents and in Radiative Forcing, in: Cli- mate Change 2007: The Physical Science Basis. Contribution of Working Group I to the Fourth Assessment Report of the Inter- governmental Panel on Climate Change, edited by: Solomon, S., Qin, D., Manning, M., Chen, Z., Marquis, M., Averyt, K. B., Tignor, M., and Miller, H. L., Cambridge University Press, Cam- bridge, UK and New York, NY, USA, 2007.

Frolking, S., et al. (2011), Peatlands in the Earth's 21st century climate system, *Environ. Rev.*, 19, 371-396, doi:10.1139/A11-014.

Giglio, L., G. R. van der Werf, J. T. Randerson, G. J. Collatz, and P. Kasibhatla, (2006), Global estimation of burned area using MODIS active fire observations, *Atmos. Chem. Phys., 6*, 957-974, 2006, doi:10.5194/acp-6-957-2006.

Gurney, K., R. Law, P. Rayner, and S. Denning, "TransCom 3 Experimental Protocol," Department of Atmospheric Science, Colorado State University, paper no. 707, July 2000.

Hansen, J. R. Ruedy, M. Sato, and K. Lo, (2010), Global surface temperature change, *Rev. Geophys., 48*, RG4004, doi:10.1029/2010RG000345.

Harden, J.W., C. Koven, C. Ping, G. Hugelius, A. D. McGuire, P. Camill, T. Jorgenson, P. Kuhry, G.J. Michaelson, J. O'Donnell, E.A. Schuur, C. Tarnocai, K. Johnson, G. Grosse, (2012), Field information links permafrost carbon to physical vulnerabilities of thawing, *Geophys. Res. Lett., 39*, L15704, doi:10.1029/2012GL051958.

Hein, R., Crutzen, P. J., and Heimann, M.: An inverse modeling approach to investigate the global atmospheric methane cycle, Global. Biogeochem. Cy., 11, 43–76, 1997.

Hofmann, D. J., J. H. Butler, E. J. Dlugokencky, J. W. Elkins, K. Masarie, S. A. Montzka, and P. Tans, (2006a), The role of carbon dioxide in climate forcing from 1979 - 2004:

Introduction of the Annual Greenhouse Gas Index, Tellus B, 58B, 614-619.

Houtekamer, P.L., and H.L. Mitchell (1998), Data assimilation using an ensemble Kalman filter technique, *Mon. Weather. Rev., 126(3)*, 796-811.

Houweling, S., Krol, M., Bergamaschi, P., Frankenberg, C., Dlugokencky, E. J., Morino, I., Notholt, J., Sherlock, V., Wunch, D., Beck, V., Gerbig, C., Chen, H., Kort, E. A., Röckmann, T., and Aben, I.: A multi-year methane inversion using SCIAMACHY, accounting for systematic errors using TCCON measurements, Atmos. Chem. Phys., 14, 3991-4012, doi:10.5194/acp-14-3991-2014, 2014.

Houweling, S., T. Kaminski, F. Dentener, J. Lelieveld, M. Heimann, (1999), Inverse modeling of methane sources and sinks using the adjoint of a global transport model, *J. Geophys. Res., 104*, D21, DOI: 10.1029/1999JD900428.

Kaminski, T., P.J. Rayner, M. Heimann, and I.G. Enting, (2001), On aggregation errors in atmospheric transport inversions, J. Geophys. Res. 106(D5), 4703-4715.

Kaplan, J. O., (2002), Wetlands at the last glacial maximum: Distribution and methane emissions, *Geophys. Res. Lett., 29(6)*, 1079, doi:10.1029/2001GL013366.

Karion, Anna, Colm Sweeney, Gabrielle Pétron, Gregory Frost, R. Michael Hardesty, Jonathan Kofler, Ben R. Miller, Tim Newberger, Sonja Wolter, Robert Banta, Alan Brewer, Ed Dlugokencky, Patricia Lang, Stephen A. Montzka, Russell Schnell, Pieter Tans, Michael Trainer, Robert Zamora and Stephen Conley, (2013), Methane emissions estimate from airborne measurements over a western United States natural gas field, *Geophysical Research Letters*, 10.1002/grl.50811.

Krol, M., S. Houweling, B. Bregman, M. van den Broek, A. Segers, P. van Velthoven, W. Peters, F. Dentener, and P. Bergamaschi, (2005), The two-way nested global chemistry-transport zoom model TM5: algorithm and applications, *Atmos. Chem. Phys., 5*, 417-432, doi:10.5194/acp-5-417-2005.

Krol, M., J. Lelieveld, (2003), Can the variability in tropospheric OH be deduced from measurements of 1,1,1-trichloroethane (methyl chloroform)?, *J. Geophys. Res., 108*, D3, DOI: 10.1029/2002JD002423.

Loulergue, L., A. Schilt, R. Spahni, V. Masson-Delmotte, T. Blunier, B. Lemieux, J.-M. Barnola, D. Raynaud, T. F. Stocker and J. Chappellaz, (2008) Orbital and millennial-scale features of atmospheric CH_4 over the past 800,000 years, *Nature, 453*, 383-386, doi10.1038/nature06950.

Masarie, K. A. and P. P. Tans, (1995), Extension and integration of atmospheric carbon dioxide data into a globally consistent measurement record, *Journal of Geophysical Research-Atmospheres*, 100, D6, 11593-11610.

Matthews, E., Fung, I., and Lerner, J.: Methane emission from rice cultivation: Geographic and seasonal distribution of cultivated areas and emissions, Global Biogeochem. Cycles, 5, 3–24, 1991.

Matthews, E., 1989: *Global Data Bases on Distribution, Characteristics and Methane Emission of Natural Wetlands: Documentation of Archived Data Tape*. NASA TM-4153. National Aeronautics and Space Administration.

McGuire, A.D., T.R. Christensen, D. Hayes, A. Heroult, E. Euskirchen, J.S. Kimball, C. Koven, P. Lafleur, P.A. Miller, W. Oechel, P. Peylin, M. Williams, and Y. Yi, (2012) An assessment of the carbon balance of Arctic tundra: comparisons among observations, process models, and atmospheric inversions, *Biogeosci., 9*, 3185-3204, doi:10.5194/bg-9-3185-2012.

Melack, J.M., L. L. Hess, M. Gastil, B. R. Forsberg, S. K. Hamilton, I. B.T. Lima and E. M.L.M. Novo, (2004), Regionalization of methane emissions in the Amazon Basin with microwave remote sensing, *Global Change Biology 10*, 530–544, doi: 10.1111/j.1529-8817.2003.00763.x.

Melton, J.R., R. Wania, E.L. Hodson, B. Poulter, B. Ringeval, R. Spahni, T. Bohn, C.A. Avis, D.J. Beerling, G. Chen, A.V. Eliseev, S.N. Denisov, P.O. Hopcroft, D.P. Lettenmaier, W.J. Riley, J.S. Singarayer, Z.M Subin, H.Tian, S. Zurcher, V. Brovkin, P.M. van Bodegom, T. Kleinen, Z.C. Yu, and J.O. Kaplan (2013), Present state of global wetland extent and wetland methane modelling: conclusions from a model intercomparison project (WETCHIMP), *Biogeosciences 10*, 753-788, doi:10.5194/bg-10-753-2013.

Miller, J. B., K.A. Mack, R. Dissly, J.W.C. White, E. J. Dlugokencky and P. P. Tans, (2002), Development of analytical methods and measurements of 13C/12C in atmospheric CH4 from the NOAA Climate Monitoring and Diagnostics Laboratory Global Air Sampling Network, *Journal of Geophysical Research-Atmospheres*, 107, d13, 4178, doi:10.1029/2001JD000630.

Miller, J. B., Gatti, L. V., D'Amelio, M. T. S., Crotwell, A., Dlugokencky, E., Bakwin, P. S., Artaxo, P., and Tans, P.: Airborne sampling reveals large methane enhancement over the Amazon basin, Geophys. Res. Lett., 34, 2007.

Miller. Scot M., Steven C. Wofsy, Anna M. Michalak, Eric A. Kort, Arlyn E. Andrews, Sebastien C. Biraud, Edward J. Dlugokencky, Janusz Eluszkiewicz, Marc L. Fischer, Greet Janssens-Maenhout, Ben R. Miller, John B. Miller, Stephen A. Montzka, Thomas Nehrkorn, and Colm Sweeney (2013), Anthropogenic emissions of methane in the United States, *PNAS 110* (50) 20018-20022, doi:10.1073/pnas.1314392110.

Mikaloff Fletcher, S. E., P. P. Tans, L. M. Bruhwiler, J. B. Miller, and M. Heimann (2004a), CH_4 sources estimated from atmospheric observations of CH_4 and its $^{13}C/^{12}C$ isotopic ratios: 1. Inverse modeling of source processes, *Global Biogeochem. Cycles, 18*, GB4004, doi:10.1029/2004GB002223.

Mikaloff Fletcher, S. E., P. P. Tans, L. M. Bruhwiler, J. B. Miller, and M. Heimann (2004b), CH_4 sources estimated from atmospheric observations of CH4 and its $^{13}C/^{12}C$ isotopic ratios: 2. Inverse modeling of CH*4* fluxes from geographical regions, *Global Biogeochem. Cycles, 18*, GB4005, doi:10.1029/2004GB002224.

Montzka, S.A., M. Krol, E. Dlugokencky, B. Hall, P. Jockel, J. Lelieveld, (2011), Small Interannual Variability of Global Atmospheric Hydroxyl, *Science, 331*, 6013, pp. 67-69, DOI: 10.1126/science.1197640.

Myhre, G., D. Shindell, F.-M. Bréon, W. Collins, J. Fuglestvedt, J. Huang, D. Koch, J.-F. Lamarque, D. Lee, B. Mendoza, T. Nakajima, A. Robock, G. Stephens, T. Takemura and H. Zhang, 2013: Anthropogenic and Natural Radiative Forcing. In: *Climate Change 2013: The Physical Science Basis. Contribution of Working Group I to the Fifth Assessment Report of the Intergovernmental Panel on Climate Change* [Stocker, T.F., D. Qin, G.-K. Plattner, M. Tignor, S.K. Allen, J. Boschung, A. Nauels, Y. Xia, V. Bex and P.M. Midgley (eds.)]. Cambridge University Press, Cambridge, United Kingdom and New York, NY, USA.

Peters, W., A.R. Jacobson, C. Sweeney, A. Andrews, T. J. Conway, K. A. Masarie, J. B. Miller, L. Bruhwiler, G. Petron, A. Hirsch, D. Worthy, G. van der Werf, J. T. Randerson, P. Wennberg, M. Krol and P. P. Tans, (2007), An atmospheric perspective on North American carbon dioxide exchange: CarbonTracker, *Proceedings of the National Academy of Sciences*, 104, 48, 18925-18930, 10.1073/pnas.0708986104.

Peters, W., J. B. Miller, J. Whitaker, A. S. Denning, A. Hirsch, M. C. Krol, D. Zupanski, L. Bruhwiler, P. P. Tans, (2005), An ensemble data assimilation system to estimate CO_2 surface fluxes from atmospheric trace gas observations, *J. Geophys. Res., 110*, D24, DOI: 10.1029/2005 JD006157.

Peters, W, M. C. Krol, E. J. Dlugokencky, F. J. Dentener, P. Bergamaschi, G. Dutton, P. v. Velthoven, J. B. Miller, L. Bruhwiler, P. P. Tans, (2004), Toward regional-scale modeling using the two-way nested global model TM5: Characterization of transport using SF_6, *J. Geophys. Res., 109*, D19, DOI: 10.1029/2004JD005020.

Pétron, Gabrielle, G. Frost, B. R. Miller, A. I. Hirsch, S. A. Montzka, A. Karion, M. Trainer, C. Sweeney, A. E. Andrews, L. Miller, J. Kofler, A. Bar-Ilan, E. J. Dlugokencky, L. Patrick, C. T. Moore Jr., T. B. Ryerson, C. Siso, W. Kolodzey, P. M. Lang, T. Conway, P. Novelli, K. Masarie, B. Hall, D. Guenther, D. Kitzis, J. Miller, D. Welsh, D. Wolfe, W. Neff, P. Tans, (2012), Hydrocarbon emissions characterization in the Colorado Front Range: A pilot study, J. Geophys. Res., v117, D4, DOI: 10.1029/2011JD016360.

Rayner, P. J., M. Scholze, W. Knorr, T. Kaminski, R. Giering, and H. Widmann (2005), Two decades of terrestrial carbon fluxes from a carbon cycle data assimilation system (CCDAS), *Global Biogeochem. Cycles, 19*, GB2026, doi:10.1029/2004GB002254.

Rhee, T.S., A.J. Kettle, and M.O. Andreae, (2009), Methane and nitrous oxide emissions from the ocean: A reassessment using basin-wide observations in the Atlantic, J. Geophys. Res., 114, D12304, doi:10.1029/2008JD011662.

Ridgwell, A. J., S. J. Marshall, K. Gregson, (1999), Consumption of atmospheric methane by soils: A process-based model, *G.B.C., 13*, 1, 59-70, DOI: 10.1029/1998GB900004.

Rigby, M., Prinn, R. G., Fraser, P. J., Simmonds, P. G., Lan- genfelds, R. L., Huang, J., Cunnold, D. M., Steele, L. P., Krummel, P. B., Weiss, R. F., O'Doherty, S., Salameh, P. K., Wang, H. J., Harth, C. M., Muhle, J., and Porter, L. W.: Re- newed growth of atmospheric methane, Geophys. Res. Lett., 35, L22805, doi:10.1029/2008gl036037, 2008.

Sanderson, M.G., (1996), Biomass of termites and their emissions of methane and carbon dioxide: A global database, *G.B.C., 10,* 4, 543-557, DOI: 10.1029/96GB01893.

Shakhova, N., I. Semilitov, I. Leifer, V. Sergienko, A., Salyuk, D. Kosmach, D. Chernykh, C. Stubbs, D. Nicolsky, V. Tumskoy, O. Gustafsson, (2013) Ebullition and storm-induced methane release from the East Siberian Arctic Shelf, *Nat. Geosci., 7*, 64-70, doi:10.1038/ngeo2007.

Schaefer, Kevin, Tingjun Zhang, Lori Bruhwiler, Andrew P. Barrett (2010) Strength and timing of the permafrost carbon feedback*, Tellus B,* 63B, 165-180,doi:10.1111/j.1600-0889.2011.00527.x, 2011.

Schuur, E.A., B. Abbott, and the Permafrost Carbon Network, (2011) High Risk of Permafrost Thaw, *Nature, 32*, vol. 480.

Spahni, R., R. Wania, L. Neef, M. van Weele, I. Pison, P. Bousquet, C. Frankenberg, P.N. Foster, F. Joos, I.C. Prentice, and P. van Velthoven, Constraining global methane emissions and uptake by ecosystems, *Biogeosciences, 8*, 1643-1665, 2011, doi:10.5194/bg-8-1643-2011.

Stroeve, J., M. Serreze, S. Drobot, S. Gearheard, M. Holland, J. Maslanik, W. Meier, T. Scambos, 2008. Arctic Sea Ice Extent Plummets in 2007. *Eos, Transactions, American Geophysical Union* 89(2): 13-14, doi:10.1029/2008EO020001.

Tarnocai, C., J. G. Canadell, E. A. G. Schuur, P. Kuhry, G. Mazhitova, and S. Zimov (2009), Soil organic carbon pools in the northern circumpolar permafrost region, *Global Biogeochem. Cycles*, 23, GB2023, doi:10.1029/2008GB003327.

Walter, B. P. and Heimann, M., A process-based, climate-sensitive model to derive methane emissions from natural wetlands: Application to five wetland sites, sensitivity to model parameters, and climate, *Global Biogeochem. Cycles*, *14,* 3, 745–765, 2000.

Walter Anthony, K., L. C. Smith and F. S. Chapin III, (2007) Methane bubbling from northern lakes: present and future contributions to the global methane budget, *Phil. Trans. R. Soc. A., 365*, 1657-1676, DOI:10.1098/rsta.2007.2036.

Walter Anthony, K., P. Anthony, G. Grosse and J. Chanton, (2012) Geologic methane seeps along boundaries of Arctic permafrost thaw and melting glaciers, *Nature GeoSci., 5*, 419-426, DOI:10.1038/NGEO1480.

van der Werf, G.R., J. T. Randerson, L. Giglio, G. J. Collatz, P. S. Kasibhatla, and A. F. Arellano, Jr., (2006), Interannual variability in global biomass burning emissions from 1997 to 2004, *Atmos. Chem. Phys., 6*, 3423–3441, www.atmos-chem-phys.net/6/3423/2006/.

Whitaker, J.S. and T.M. Hamill, (2002), Ensemble Data Assimilation without Perturbed Observations, *Mon. Wea. Rev.*, **130**, 1913–1924, doi: http://dx.doi.org/10.1175 /1520-0493(2002) 130<1913:EDAWPO>2.0.CO;2.

Yan X., H. Akiyama, K. Yagi, H. Akimoto, (2009), Global estimations of the inventory and mitigation potential of methane emissions from rice cultivation conducted using the 2006 Intergovernmental Panel on Climate Change Guidelines, *G.B.C., 23,* 2, DOI: 10.1029/2008GB003299.

Shakhova, N., I. Semilitov, A. Salyuk, V. Yusupov, D. Kosmach, O. Gustafsson, (2010) Extensive venting the atmosphere from sediments of the East Siberian Arctic shelf, *Science, 5,* Vol. 327 no. 5970 pp. 1246-1250 DOI: 10.1126/science.1182221.

Schaefer, Kevin, Tingjun Zhang, Lori Bruhwiler, Andrew P. Barrett (2010) Strength and timing of the permafrost carbon feedback*, Tellus B,* 63B, 165-180,doi:10.1111/j.1600-0889.2011.00527.x, 2011.

Schuur, E.A., B. Abbott, and the Permafrost Carbon Network, (2011) High Risk of Permafrost Thaw, *Nature, 32*, vol. 480.

Spahni, R., R. Wania, L. Neef, M. van Weele, I. Pison, P. Bousquet, C. Frankenberg, P.N. Foster, F. Joos, I.C. Prentice, and P. van Velthoven, Constraining global methane emissions and uptake by ecosystems, *Biogeosciences, 8*, 1643-1665, 2011, doi:10.5194/bg-8-1643-2011.

Stroeve, J., M. Serreze, S. Drobot, S. Gearheard, M. Holland, J. Maslanik, W. Meier, T. Scambos, 2008. Arctic Sea Ice Extent Plummets in 2007. *Eos, Transactions, American Geophysical Union* 89(2): 13-14, doi:10.1029/2008EO020001.

Tarnocai, C., J. G. Canadell, E. A. G. Schuur, P. Kuhry, G. Mazhitova, and S. Zimov (2009), Soil organic carbon pools in the northern circumpolar permafrost region, *Global Biogeochem. Cycles*, 23, GB2023, doi:10.1029/2008GB003327.

Walter, B. P. and Heimann, M., A process-based, climate-sensitive model to derive methane emissions from natural wetlands: Application to five wetland sites, sensitivity to model parameters, and climate, *Global Biogeochem. Cycles*, *14,* 3, 745–765, 2000.

Walter Anthony, K., L. C. Smith and F. S. Chapin III, (2007) Methane bubbling from northern lakes: present and future contributions to the global methane budget, *Phil. Trans. R. Soc. A., 365*, 1657-1676, DOI:10.1098/rsta.2007.2036.

Walter Anthony, K., P. Anthony, G. Grosse and J. Chanton, (2012) Geologic methane seeps along boundaries of Arctic permafrost thaw and melting glaciers, *Nature GeoSci., 5*, 419-426, DOI:10.1038/NGEO1480.

van der Werf, G.R., J. T. Randerson, L. Giglio, G. J. Collatz, P. S. Kasibhatla, and A. F. Arellano, Jr., (2006), Interannual variability in global biomass burning emissions from 1997 to 2004, *Atmos. Chem. Phys., 6*, 3423–3441, www.atmos-chem-phys.net/6/3423/2006/.

Whitaker, J.S. and T.M. Hamill, (2002), Ensemble Data Assimilation without Perturbed Observations, *Mon. Wea. Rev.*, **130**, 1913–1924, doi: http://dx.doi.org/10.1175 /1520-0493(2002) 130<1913:EDAWPO>2.0.CO;2.

Yan X., H. Akiyama, K. Yagi, H. Akimoto, (2009), Global estimations of the inventory and mitigation potential of methane emissions from rice cultivation conducted using the 2006 Intergovernmental Panel on Climate Change Guidelines, *G.B.C., 23,* 2, DOI: 10.1029/2008GB003299.

Table 1 – CarbonTracker-CH_4 data preprocessing.

Measurement Program	Data Preprocessing
ESRL discrete surface	All valid* data. Multiple values from the same day and location are averaged. No sample time-of-day restriction (see exception below).
EC in situ sites	All valid data from highest intake. Day average using 12-16 LST.

* In this context "Valid Data" means the observation is thought to be free of sampling and analytical problems and has not been locally influenced.

Table 2- Summary of the observation sites used in CarbonTracker-CH4, and the performance of the assimilation scheme at each site. “#Obs.” and “#Rej.” are the number of observations available and the number of observations for which the prior simulated concentrations deviate more than 3σ from the observations using a normal distribution defined with the observed value as the mean and the model-data mismatch error (MDM) as the standard deviation. The bias is the long-term mean of the posterior residuals (simulated-observed), σ is the standard deviation of the residuals for each site, and C2 is the chi-squared statistic calculated as the mean residual divided by the prior uncertainty (Simulated-Observed/(HQH+R); where H is the matrix of transport response, Q is the prior flux uncertainty and R is the model-data mismatch error).

Site Code	Lab	Lat.	Lon.	Elev. masl	# Obs.	# Rej.	MDM ppb	Bias ppb	σ ppb	χ2
abp_01d0	ESRL	12.77S	38.17W	1.0	112	3	7.5	-8.4	7.7	2.0
alt_01d0	ESRL	82.45N	62.51W	200.0	532	0	15.0	-2.2	8.7	0.3
alt_06c0	EC	82.45N	62.51W	200.0	3181	10	15.0	-1.2	10.2	0.4
amt_01d0	ESRL	45.03N	68.68W	50.0	267	4	30.0	-6.1	22.8	0.4
amt_01p0	ESRL	45.03N	68.68W	50.0	174	0	30.0	0.8	16.5	0.3
asc_01d0	ESRL	7.97S	14.4W	74.5	961	79	7.5	-10.0	9.3	3.0
ask_01d0	ESRL	23.18N	5.42E	2728.0	491	0	25.0	-6.9	9.1	0.2
azr_01d0	ESRL	38.77N	27.38W	40.0	350	16	15.0	-12.0	15.9	1.7
bal_01d0	ESRL	55.35N	17.22E	3.0	974	0	75.0	1.4	29.4	0.1
bhd_01d0	ESRL	41.41S	174.87E	85.0	165	0	7.5	-4.1	5.4	0.7
bkt_01d0	ESRL	0.2S	100.32E	864.5	345	0	75.0	6.8	30.8	0.2
bme_01d0	ESRL	32.37N	64.65W	30.0	256	14	15.0	-13.6	17.4	2.1

bmw_01d0	ESRL	32.27N	64.88W	30.0	352	7	15.0	-13.2	12.8	1.4
brw_01d0	ESRL	71.32N	156.61W	11.0	514	13	15.0	-5.8	16.1	1.1
bsc_01d0	ESRL	44.17N	28.68E	3.0	501	1	75.0	-14.4	56.2	0.5
cba_01d0	ESRL	55.21N	162.72W	21.34	892	23	15.0	-10.6	13.4	1.1
cdl_06c0	EC	53.99N	105.12W	600.0	1390	77	25.0	-24.7	30.3	2.1
cgo_01d0	ESRL	40.68S	144.69E	94.0	416	0	7.5	-4.1	4.6	0.6
chr_01d0	ESRL	1.7N	157.17W	3.0	426	79	7.5	-14.6	9.9	5.2
crz_01d0	ESRL	46.45S	51.85E	120.0	453	0	7.5	-2.9	4.3	0.5
egb_06c0	EC	44.23N	79.78W	251.0	1810	0	75.0	-6.9	28.7	0.1
eic_01d0	ESRL	27.15S	109.45W	50.0	323	3	7.5	-7.3	5.3	1.4
esp_06c0	EC	49.58N	126.37W	7.0	403	0	25.0	-6.8	12.3	0.3
etl_06c0	EC	54.35N	104.98W	492.0	1780	135	25.0	-30.1	31.9	2.8
fsd_06c0	EC	49.88N	81.57W	210.0	3409	10	25.0	-9.4	18.3	0.6
gmi_01d0	ESRL	13.43N	144.78E	3.0	802	11	15.0	-10.2	13.0	1.2
hba_01d0	ESRL	75.58S	26.5W	30.0	506	0	7.5	0.5	4.6	0.3
hpb_01d0	ESRL	47.8N	11.01E	985.0	241	17	25.0	-13.8	35.7	1.4
hun_01d0	ESRL	46.95N	16.65E	248.0	530	3	75.0	-14.0	43.7	0.3
ice_01d0	ESRL	63.4N	20.29W	118.0	529	7	15.0	-3.3	13.1	0.6
izo_01d0	ESRL	28.31N	16.5W	2360.0	443	2	15.0	-8.5	11.4	0.9
key_01d0	ESRL	25.67N	80.16W	3.0	388	3	25.0	-7.0	20.1	0.6
kum_01d0	ESRL	19.52N	154.82W	3.0	720	42	7.5	-6.8	10.6	2.2
kzd_01d0	ESRL	44.06N	76.82E	601.0	454	4	75.0	5.2	44.0	0.2
kzm_01d0	ESRL	43.25N	77.88E	2519.0	447	2	25.0	-2.8	20.2	0.6
lef_01d0	ESRL	45.95N	90.27W	472.0	505	6	30.0	-9.7	28.6	0.8

lef_01p0	ESRL	45.95N	90.27W	472.0	341	7	30.0	-2.1	30.9	0.9
llb_06c0	EC	54.95N	112.45W	540.0	1152	84	75.0	-79.9	122.4	3.7
lln_01d0	ESRL	23.47N	120.87E	2862.0	222	1	25.0	-4.1	24.4	0.9
lmp_01d0	ESRL	35.52N	12.62E	45.0	206	1	25.0	-0.7	20.5	0.5
mhd_01d0	ESRL	53.33N	9.9W	5.0	416	0	25.0	-4.6	11.4	0.2
mid_01d0	ESRL	28.21N	177.38W	3.7	525	5	15.0	-10.7	10.9	1.0
mkn_01d0	ESRL	0.05S	37.3E	3897.0	146	0	25.0	-14.3	14.8	0.7
mlo_01d0	ESRL	19.54N	155.58W	3397.0	565	0	15.0	-2.4	10.9	0.5
nmb_01d0	ESRL	23.58S	15.03E	456.0	164	0	25.0	-7.8	11.4	0.3
nwr_01d0	ESRL	40.05N	105.58W	3523.0	543	18	15.0	-11.1	15.2	1.5
oxk_01d0	ESRL	50.03N	11.8E	1022.0	202	2	75.0	-12.5	42.9	0.3
pal_01d0	ESRL	67.97N	24.12E	560.0	377	54	15.0	16.7	35.1	0.2
poc000_01d1	ESRL	0.0N	155.0W	10.0	173	33	7.5	-13.9	9.5	4.7
pocn05_01D1	ESRL	5.0N	151.0W	10.0	174	29	7.5	-15.1	9.5	5.3
pocn10_01D1	ESRL	10.0N	149.0W	10.0	174	45	7.5	-16.0	14.0	7.6
pocn15_01D1	ESRL	15.0N	145.0W	10.0	168	26	7.5	-11.0	11.1	4.1
pocn20_01D1	ESRL	20.0N	141.0W	10.0	166	13	7.5	-6.8	11.5	2.9
pocn25_01D1	ESRL	25.0N	139.0W	10.0	155	14	7.5	-7.0	11.2	2.6
pocn30_01D1	ESRL	30.0N	135.0W	10.0	153	18	7.5	-4.7	13.9	2.7
pocn35_01D1	ESRL	35.0N	137.0W	10.0	5	0	7.5	-4.0	8.6	1.4
pocs05_01D1	ESRL	5.0S	159.0W	10.0	159	31	7.5	-15.3	8.6	5.2
pocs10_01D1	ESRL	10.0S	161.0W	10.0	170	41	7.5	-14.6	10.1	5.4
pocs15_01D1	ESRL	15.0S	171.0W	10.0	163	15	7.5	-10.4	9.5	3.4
pocs20_01D1	ESRL	20.0S	174.0W	10.0	169	8	7.5	-7.3	7.9	2.0

pocs25_01D1	ESRL	25.0S	171.0W	10.0	164	0	7.5	-5.3	6.3	1.1
pocs30_01D1	ESRL	30.0S	176.0W	10.0	166	0	7.5	-5.0	5.0	0.8
pocs35_01D1	ESRL	35.0S	180.0E	10.0	14	1	7.5	-0.5	8.2	0.5
psa_01d0	ESRL	64.92S	64.0W	10.0	542	0	7.5	-2.7	3.7	0.3
pta_01d0	ESRL	38.95N	123.74W	17.0	427	1	25.0	-4.6	16.9	0.4
rpb_01d0	ESRL	13.17N	59.43W	45.0	519	2	15.0	-10.7	10.0	0.9
sct_01p0	ESRL	33.41N	81.83W	115.2	351	0	75.0	-23.5	33.7	0.3
sey_01d0	ESRL	4.67S	55.17E	3.0	514	43	7.5	-6.5	12.3	3.1
sgp_01d0	ESRL	36.8N	97.5W	314.0	443	10	75.0	-56.1	57.4	0.8
shm_01d0	ESRL	52.72N	174.1E	40.0	482	0	25.0	-8.7	11.4	0.3
smo_01d0	ESRL	14.25S	170.56W	42.0	568	70	7.5	-10.5	9.9	3.6
spo_01d0	ESRL	89.98S	24.8W	2810.0	566	0	7.5	-4.1	4.7	0.7
stm_01d0	ESRL	66.0N	2.0E	0.0	917	9	15.0	-1.4	13.5	0.5
sum_01d0	ESRL	72.58N	38.48W	3238.0	468	0	15.0	-4.7	8.4	0.4
syo_01d0	ESRL	69.0S	39.58E	11.0	260	0	7.5	-2.6	3.6	0.3
tap_01d0	ESRL	36.73N	126.13E	20.0	441	3	75.0	10.2	61.7	0.5
tdf_01d0	ESRL	54.87S	68.48W	20.0	206	0	7.5	-4.2	4.1	0.6
thd_01d0	ESRL	41.05N	124.15W	107.0	400	0	25.0	-7.0	14.6	0.4
uta_01d0	ESRL	39.9N	113.72W	1320.0	525	12	25.0	-5.5	28.7	0.4
uum_01d0	ESRL	44.45N	111.1E	914.0	533	1	25.0	-1.2	22.7	0.3
wbi_01p0	ESRL	41.72N	91.35W	241.7	296	12	30.0	-8.3	38.0	1.4
wgc_01p0	ESRL	38.27N	121.49W	0.0	339	53	75.0	-118.	158.8	6.9
wis_01d0	ESRL	31.13N	34.88E	400.0	552	3	25.0	-6.2	23.7	0.8
wkt_01d0	ESRL	31.31N	97.33W	251.0	409	55	30.0	-48.6	43.7	3.8

wkt_01p0	ESRL	31.31N	97.33W	251.0	298	38	30.0	-46.7	58.7	5.8
wlg_01d0	ESRL	36.29N	100.9E	3810.0	462	17	15.0	-1.8	20.6	0.8
wsa_06c0	EC	49.93N	60.02W	5.0	2314	52	25.0	3.8	25.5	0.9
zep_01d0	ESRL	78.9N	11.88E	475.0	588	11	15.0	2.2	14.2	0.5

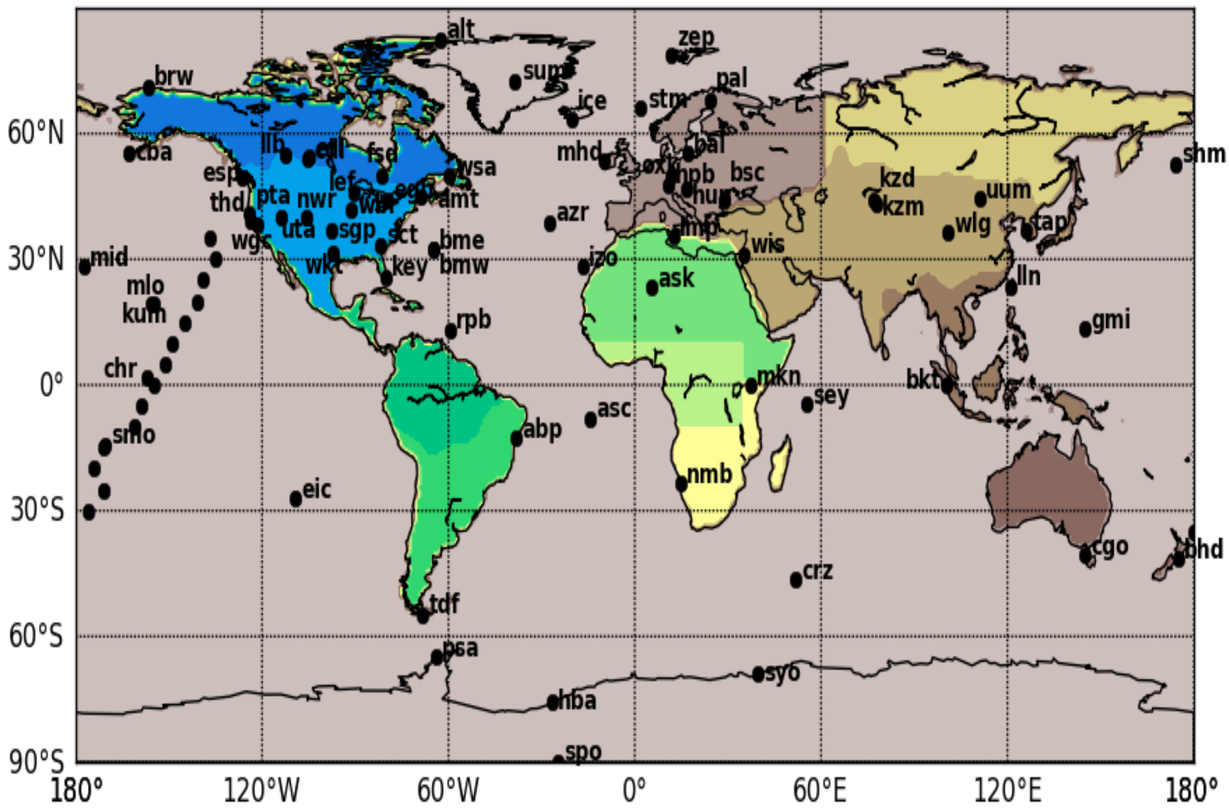

Figure 1 - Map showing locations of observations used in CarbonTracker-CH_4. Shading indicates the boundaries of the Transcom 3 source regions (Gurney et al., 2000) with an additional tropical African region.

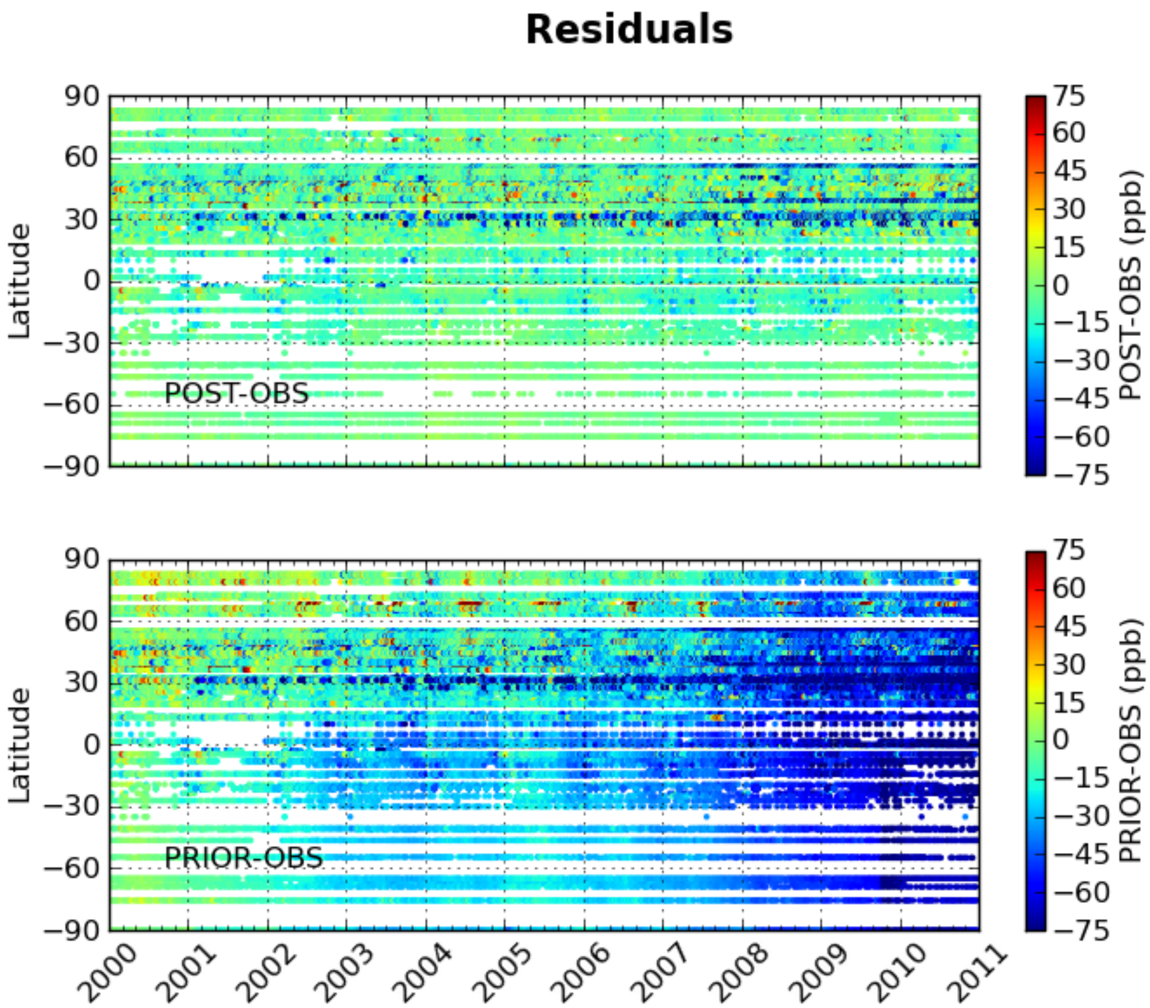

Figure 2 - The CarbonTracker posterior residuals (simulated minus observed, in nmol mol-1) as a function of time and latitude (top) and prior residuals (bottom). Each dot represents the time and location of a CH_4 observation that was assimilated in CarbonTracker. Colors represent the difference between the final simulated value and the actual measurement, with warm colors indicating that CarbonTracker simulates too much methane compared to observations, and cool colors indicating that CarbonTracker estimates too little.

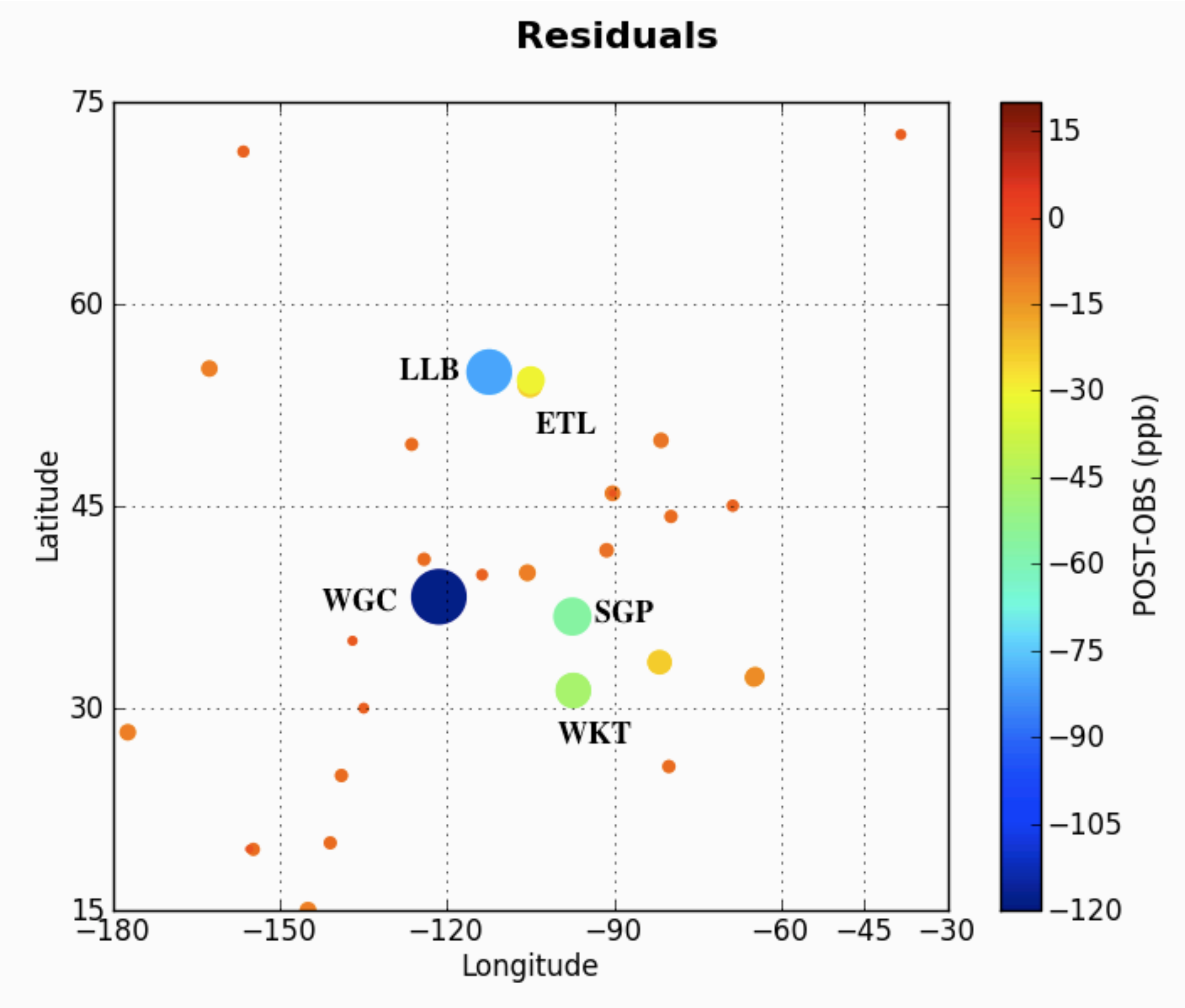

Figure 3 - The CarbonTracker posterior residuals (simulated minus observed, in nmol mol-1) as a function of time and latitude for North America. Each bubble has a radius proportional to the size of the residual, and the values are also indicated by the color bar. The largest residuals found by CarbonTracker-CH_4 are labeled also by site code.

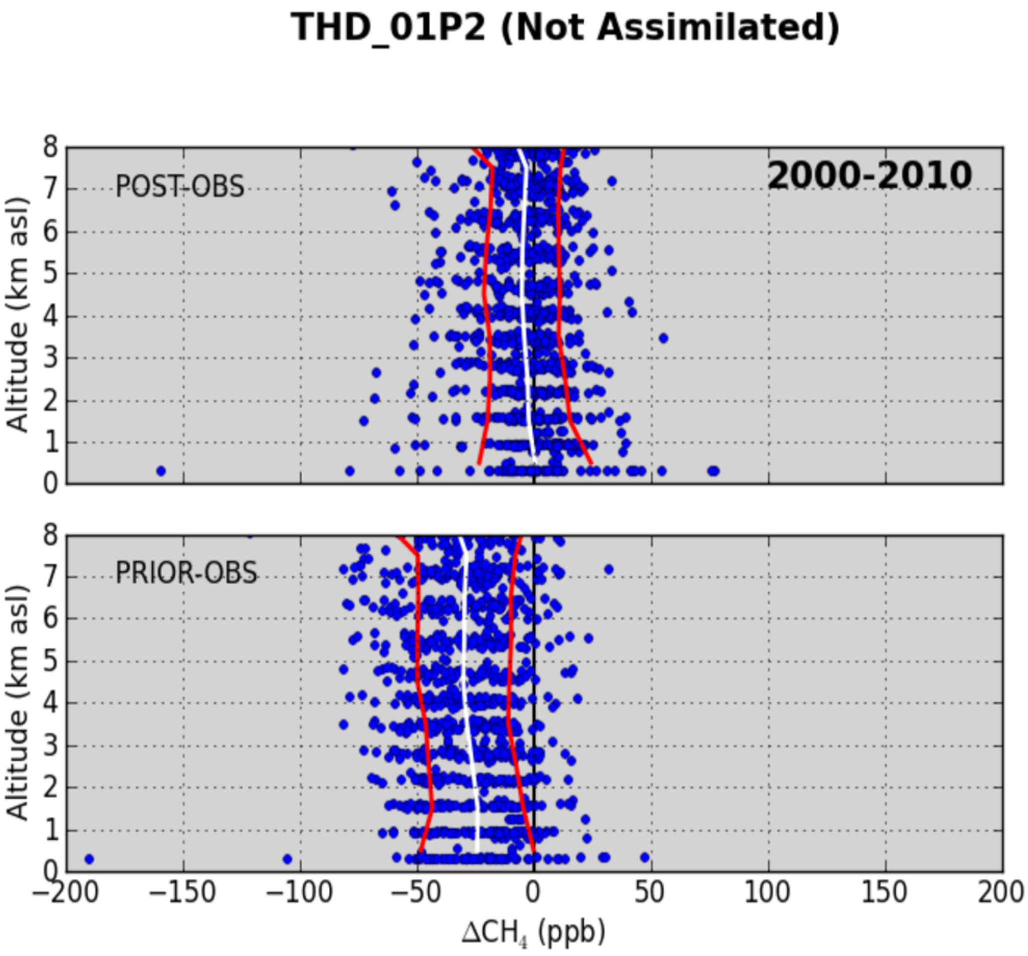

Figure 4 - Statistical summary of residuals for aircraft profiles at a site sampling marine air (Trinidad Head, CA). Units are 10^{-9} mol mol^{-1} of CH_4 (ppb). The top figure shows the post-assimilation residuals (posterior-observed) and the bottom figure shows the residuals with no data assimilation (prior-observed). Aircraft data are not currently assimilated in CarbonTracker so they provide an independent evaluation of the data assimilation. Ideally, the mean of the residuals for the simulations with data assimilation should be near zero. The residuals for the simulations without data assimilation, on the other hand, tend to show large biases.

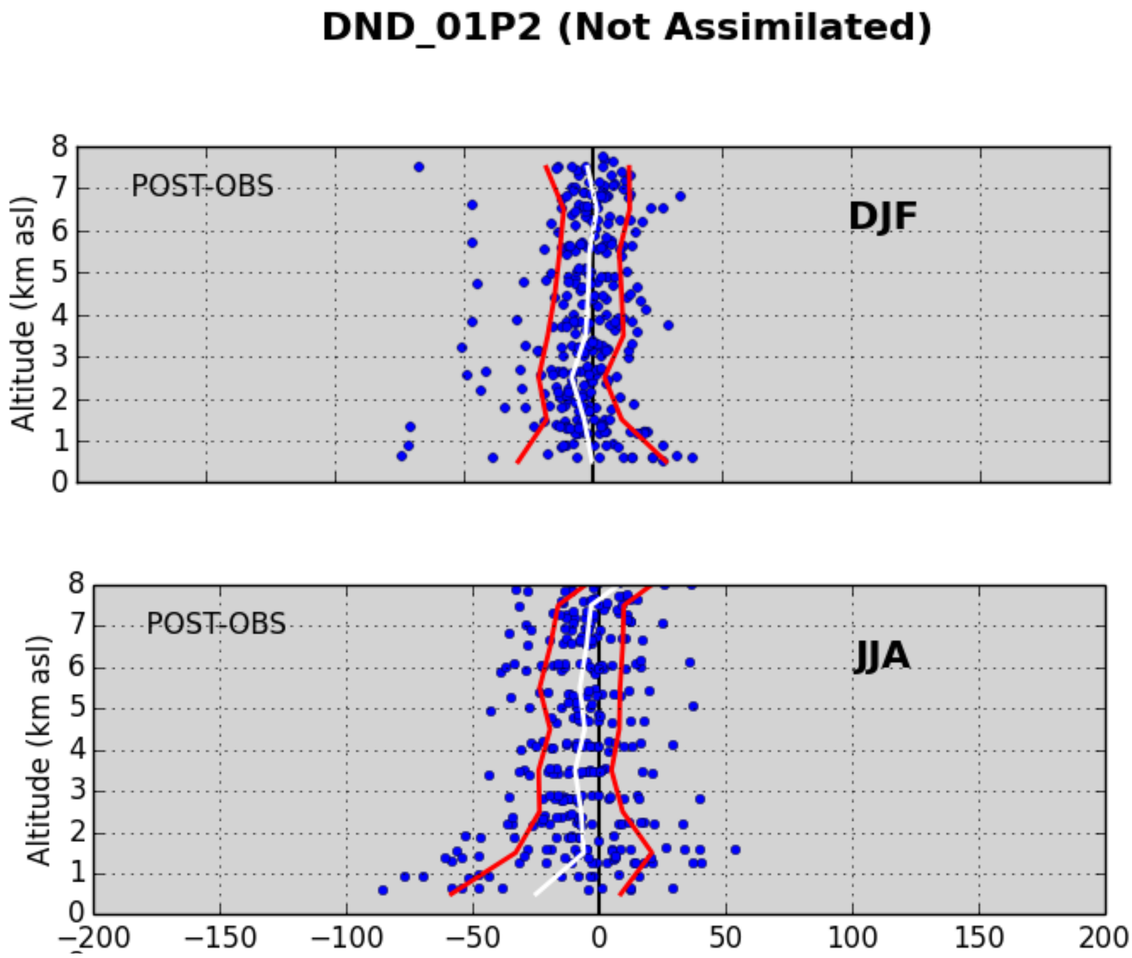

Figure 5 - Statistical summary of residuals for aircraft profiles at a site sampling continental air (Dahlen, ND; 47.5N, 99.2W). Units are 10^{-9} mol mol^{-1} of CH_4 (ppb). The top figure shows the post-assimilation residuals (posterior-observed) for winter months and the bottom figure shows the post-assimilation residuals for summer months. Note that summertime emissions near the surface are underestimated. Aircraft data are not currently assimilated in CarbonTracker so they provide an independent evaluation of the data assimilation. Ideally, the mean of the residuals for the simulations with data assimilation should be near zero. The residuals for the simulations without data assimilation, on the other hand, tend to show large biases.

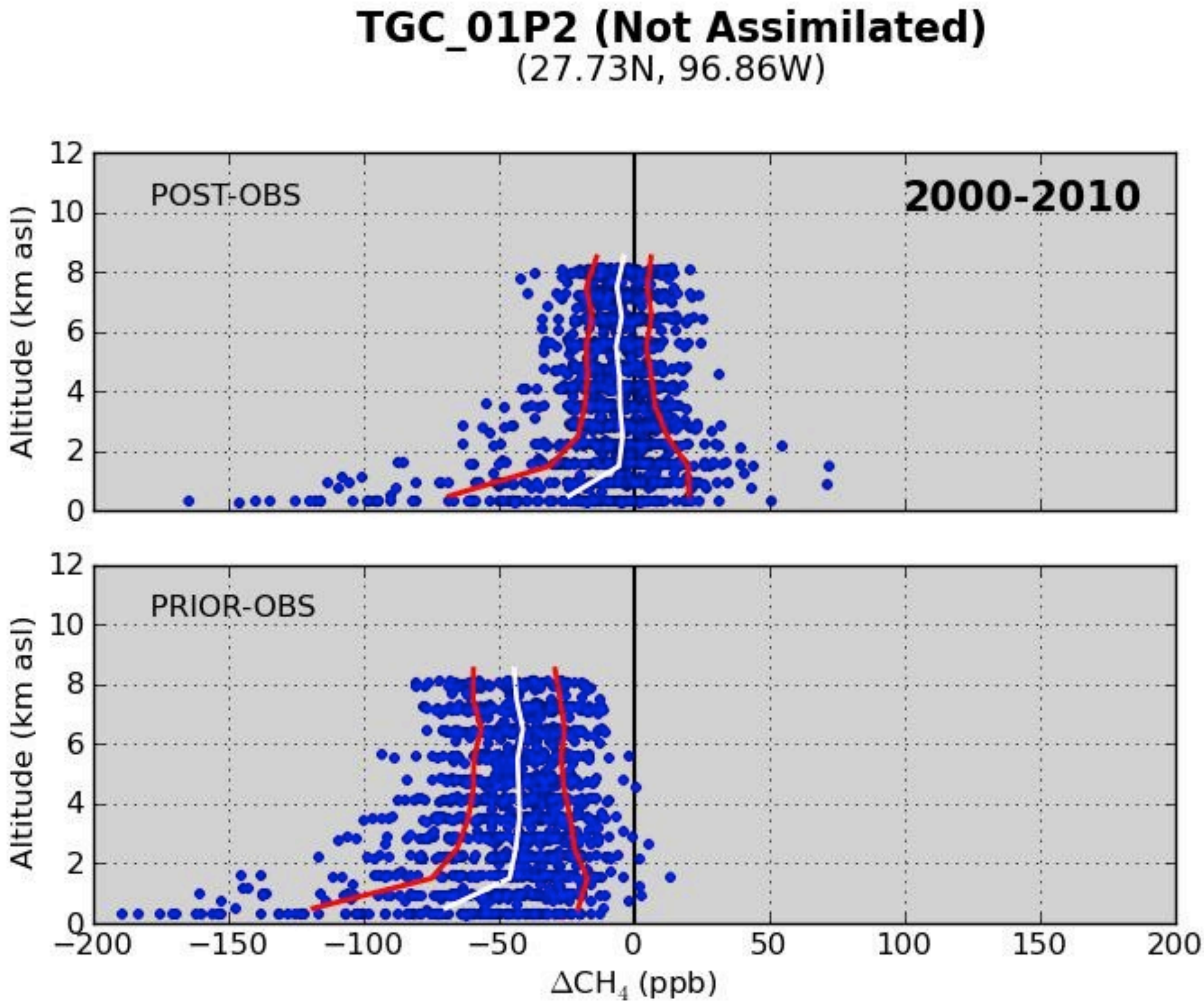

Figure 6 - Statistical summary of residuals for aircraft profiles at a site sampling continental and marine air near strong local sources. Units are 10^{-9} mol mol^{-1} of CH_4 (ppb). The top figure shows the post-assimilation residuals (posterior-observed) for and the bottom figure shows the pre-assimilation residuals (prior-observed). The mean of the residuals for the simulations with data assimilation should be near zero. The residuals for the simulations without data assimilation, on the other hand, tend to show large biases.

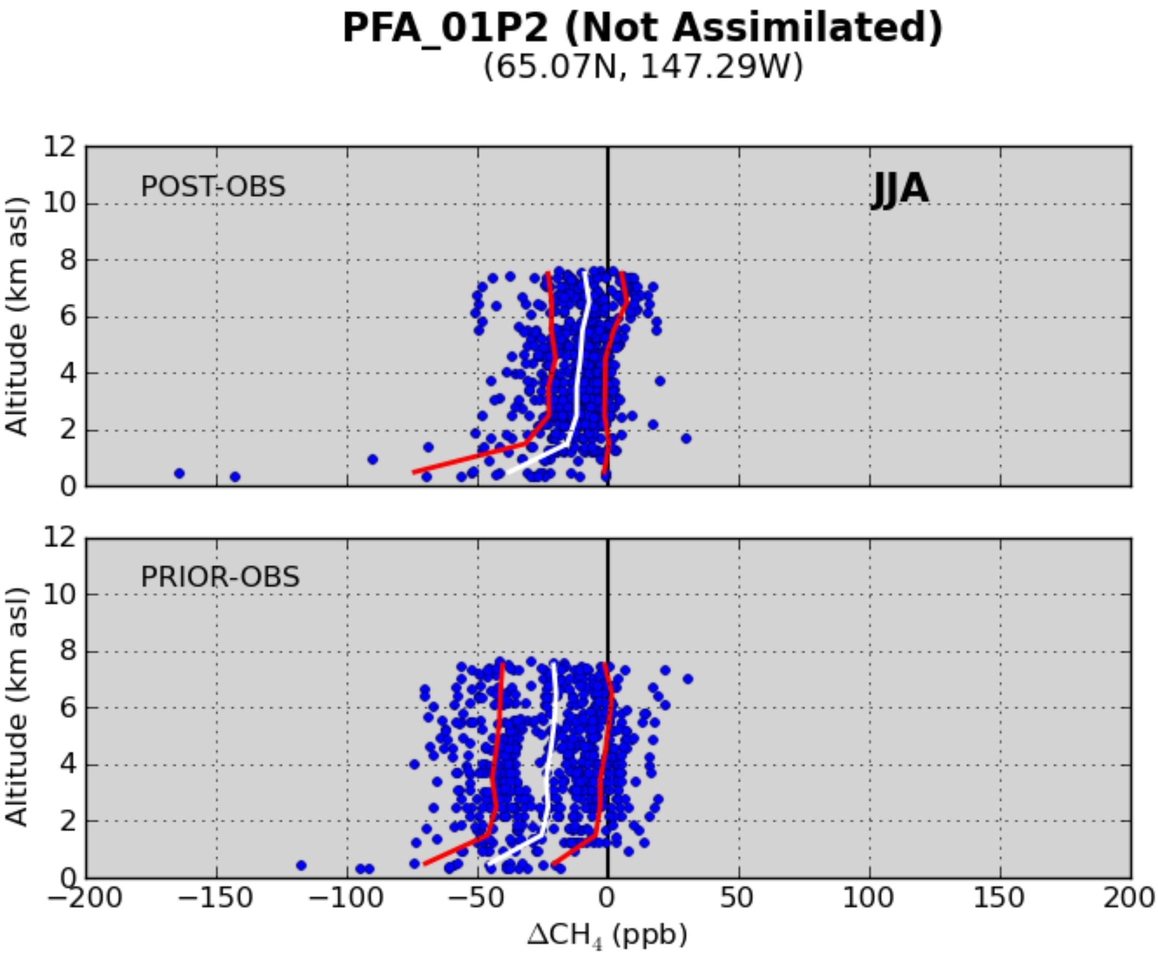

Figure 7 - Statistical summary of residuals for aircraft profiles at a high latitude site in Alaska during boreal summer. Units are 10^{-9} mol mol^{-1} of CH_4 (ppb). The top figure shows the post-assimilation residuals (posterior-observed) for and the bottom figure shows the pre-assimilation residuals (prior-observed). The mean of the residuals for the simulations with data assimilation should be near zero. The residuals for the simulations without data assimilation, on the other hand, tend to show large biases.

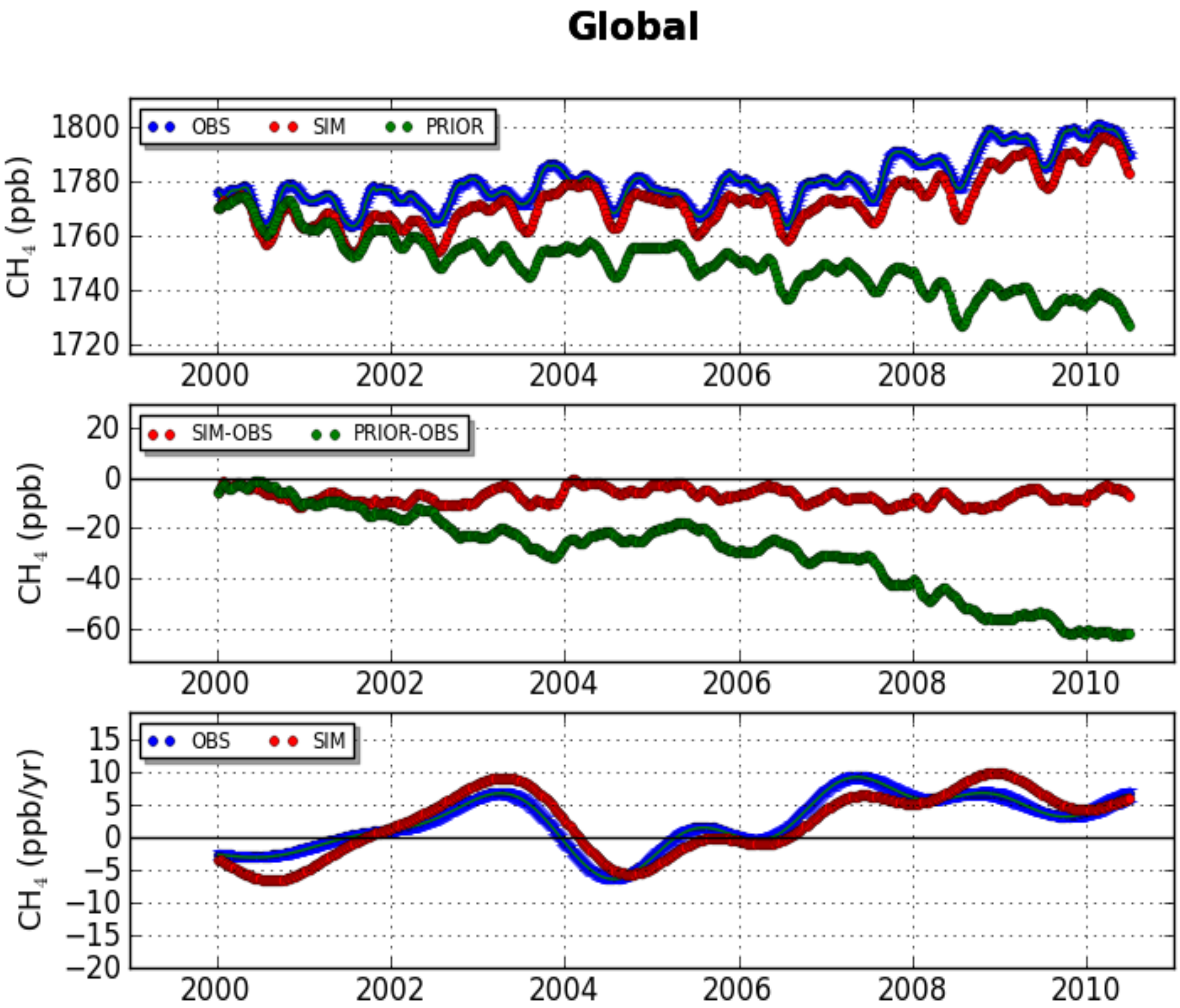

Figure 8 - (*Top*) De-seasonalized time series of observed (dark blue, "OBS", with very small error bars estimated using a bootstrap technique), assimilated (red, "SIM") and prior (green, "PRIOR") average methane mole fraction. For the "PRIOR" simulations, prior fluxes were used to calculate CH_4 mole fractions, while for the "SIM" simulations CH_4 was calculated using fluxes that were adjusted for optimal agreement with atmospheric observations. Units are ppb (10^{-9} mol mol^{-1}). *(Middle)* The differences from observations for assimilated and prior CH_4 (ppb). (*Bottom*) Derived growth rate of CH_4 mole fraction for observed (with error bars) and assimilated CH_4 mole fraction. The growth rate is computed by taking the first derivative of the average mole fractions shown in the top figure. Units are ppb yr^{-1} (10^{-9} mol mol^{-1} yr^{-1}).

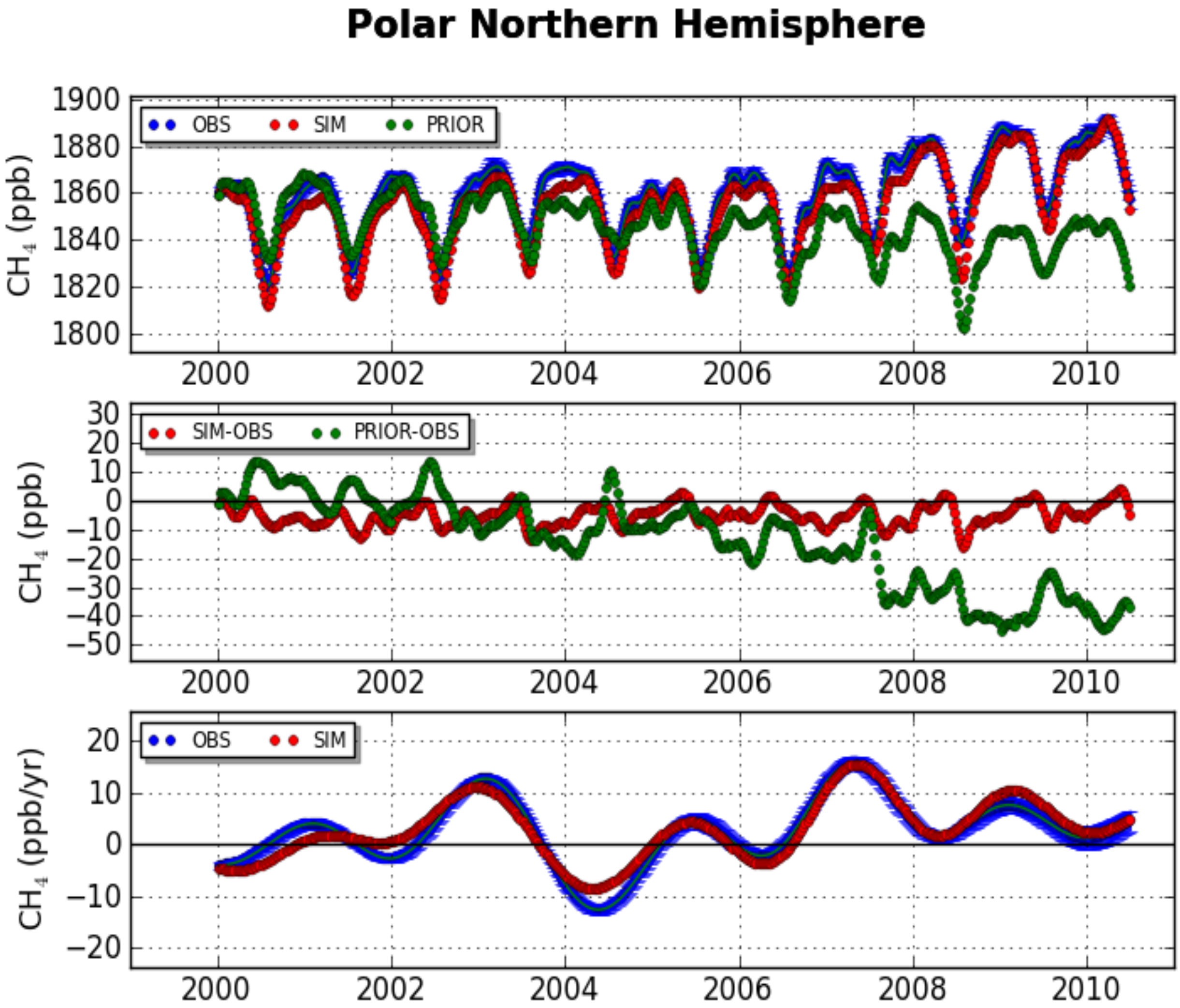

Figure 9: (*Top*) De-seasonalized time series of observed (dark blue, "OBS" with error bars), assimilated (red, "SIM") and prior (green, "PRIOR") average methane mole fraction for the Polar Northern Hemisphere (53N-90N). *(Middle)* Differences from observations for assimilated and prior CH_4 (ppb). (*Bottom*) Derived growth rate of CH_4 mole fraction for observed and assimilated CH_4 mole fraction for the Polar Northern Hemisphere.

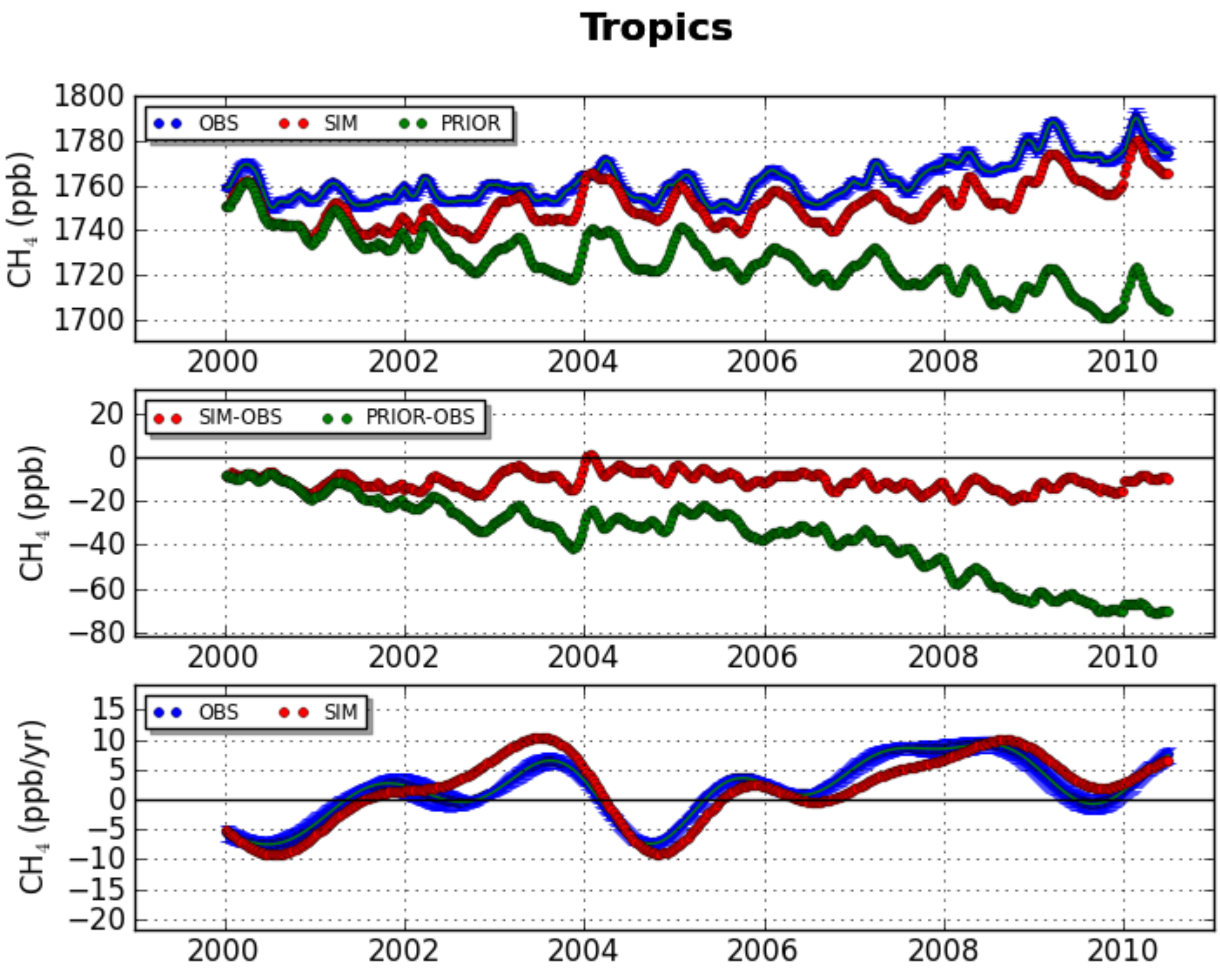

Figure 10: (*Top*) Time series of observed (dark blue, "OBS"), assimilated (red, "SIM") and prior (green, "PRIOR") average methane mole fraction for the Tropics (17.5S-17.5N). *(Middle)* Differences from observations for assimilated and prior CH_4 (ppb). (*Bottom*) Derived growth rate of CH_4 mole fraction for observed (with error bars) and assimilated CH_4 mole fraction for the Tropics.

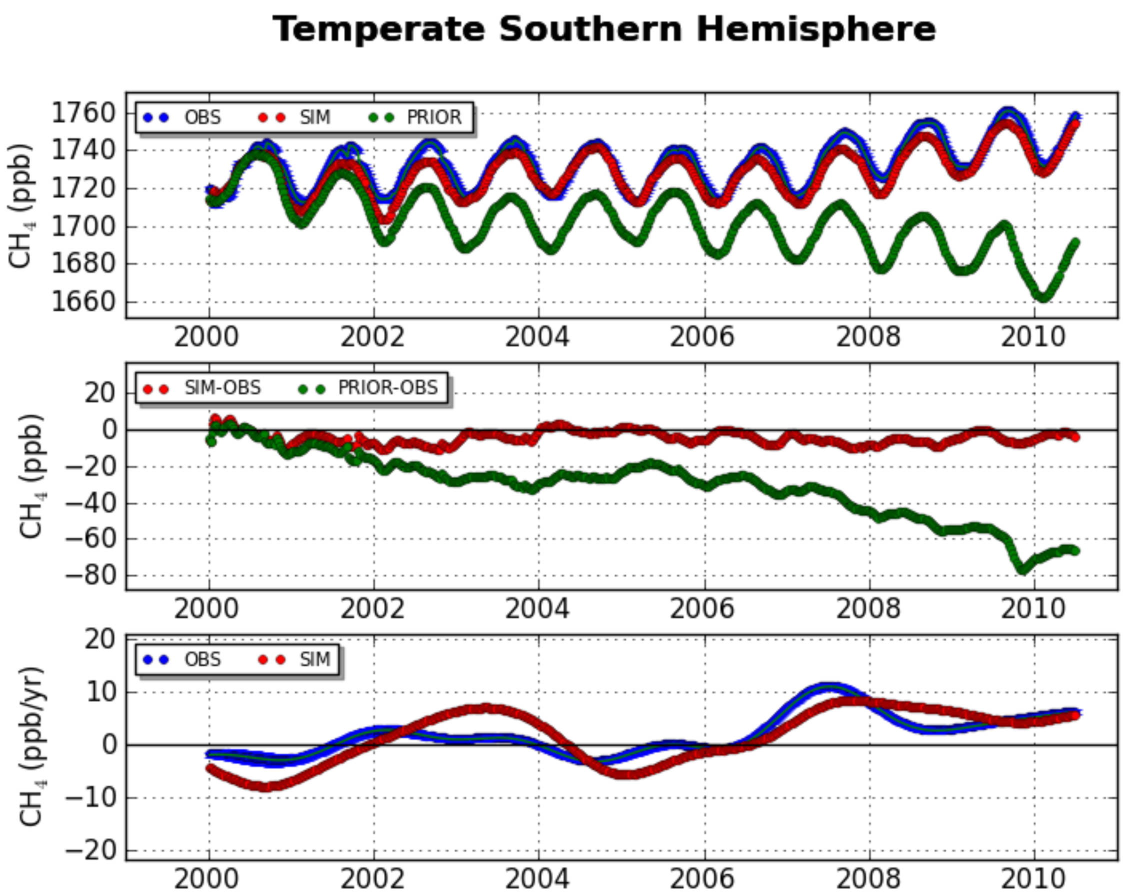

Figure 11: (*Top*) Time series of observed (dark blue, "OBS"), assimilated (red, "SIM") and prior (green, "PRIOR") average methane mole fraction for the Temperate Souther Hemisphere (17.5S-53.3S). *(Middle)* Differences from observations for assimilated and prior CH_4 (ppb). (*Bottom*) Derived growth rate of CH_4 mole fraction for observed (with error bars) and assimilated CH_4 mole fraction for the Tropics.

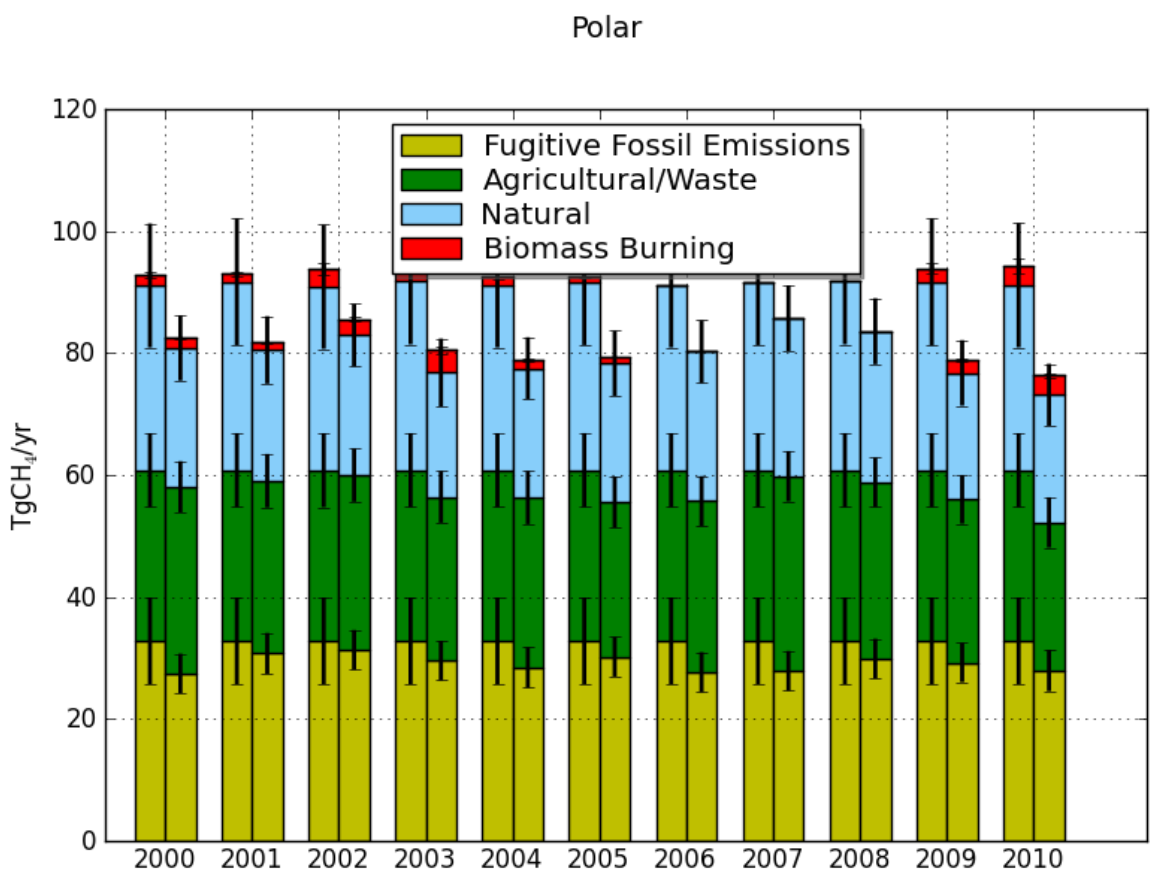

Figure 12 - The contribution to the High Northern Latitude total CH_4 flux from each category of emissions with 1-σ error estimates. For each pair of histogram bars, the prior flux estimates are shown on the left and the posterior estimates on the right. Note that, except for emissions from fires, the prior flux estimates are constant for each year. The units are Tg CH_4 yr^{-1}. The average estimated uncertainty on the total emissions is 7.5 Tg CH_4 yr^{-1}.

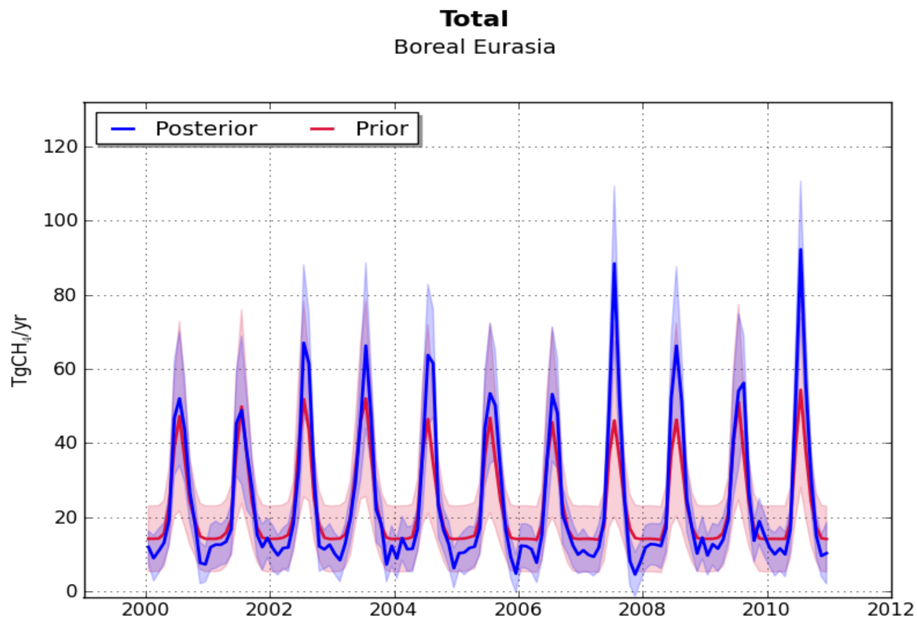

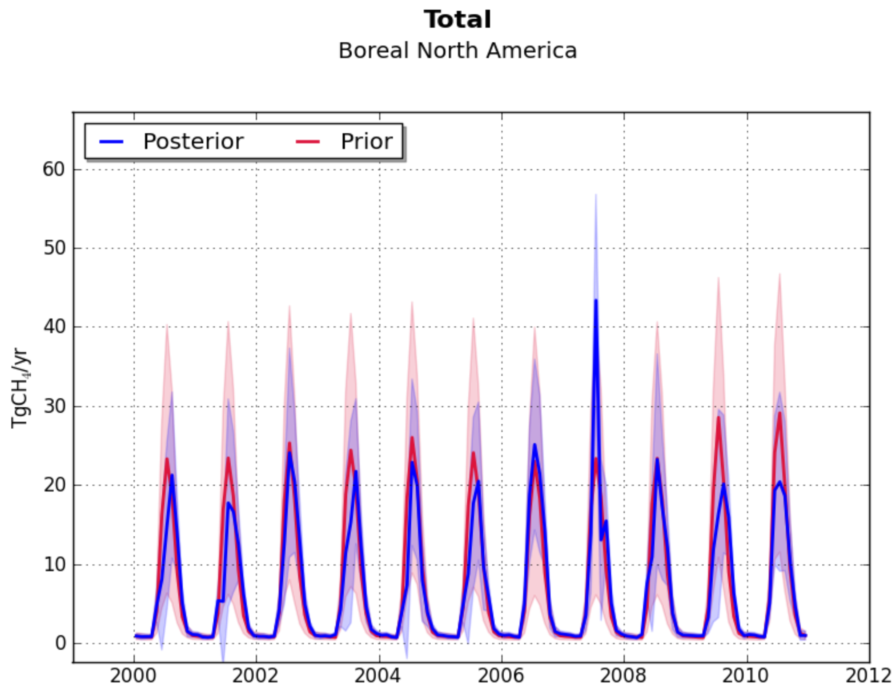

Figure 13 – Time variation of the prior and estimated CH_4 emissions. Prior estimates are shown in red, and posterior flux estimates are shown in blue. Note that only the biomass burning prior emission estimates vary from year to year; other prior estimates are constant. 1σ uncertainty bounds are shown as light red (prior) and light blue (post-assimilation) shaded areas. Note that microbial sources of methane, such as wetlands and agriculture, are temperature-sensitive and therefore tend to be largest during summer. Units are Tg CH_4 yr^{-1}.

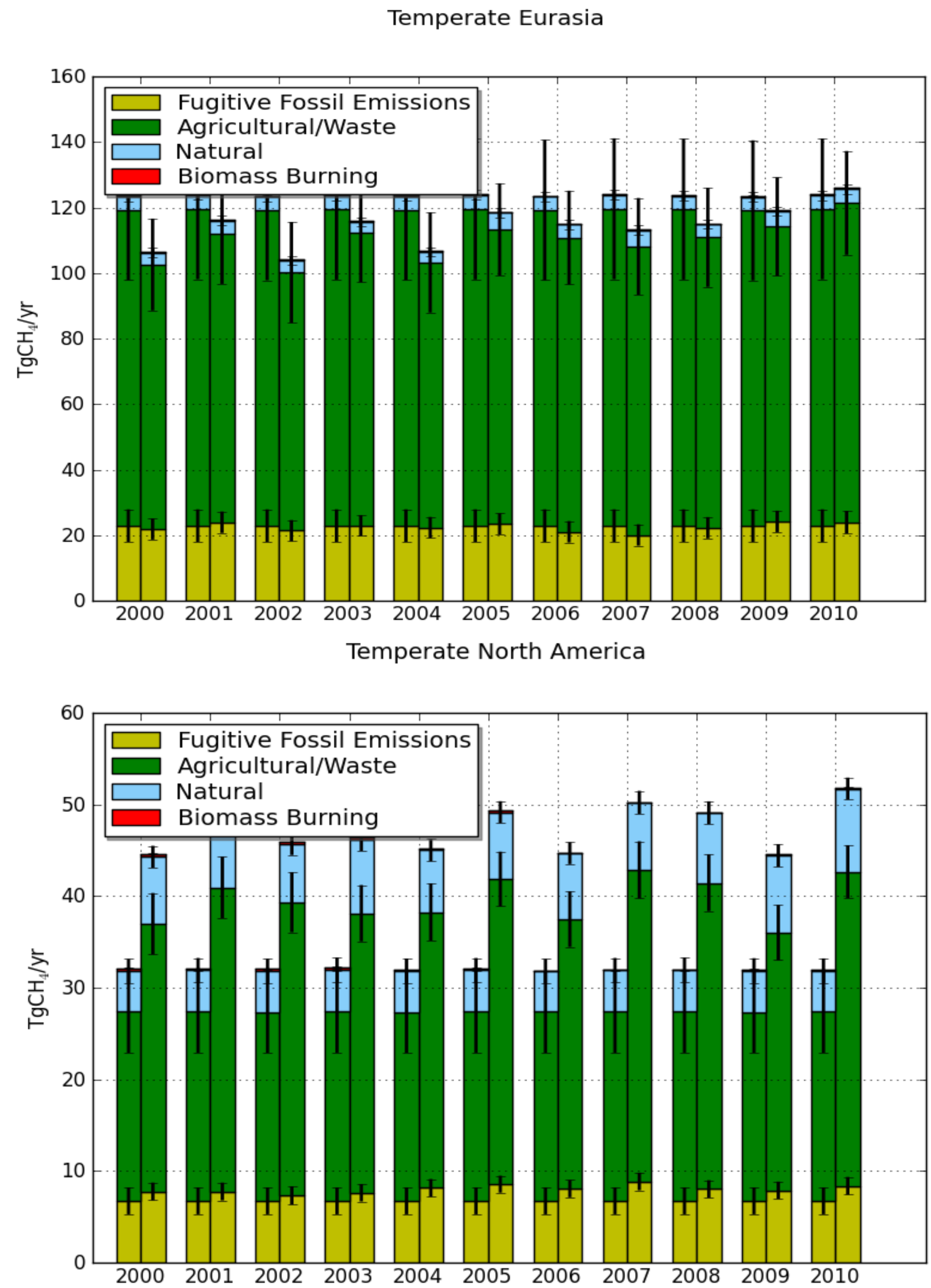

Figure 14 - The contribution to the total CH_4 flux from each category of emissions with 1-σ error bars for Temperate Eurasia (*top*) and Temperate North America (*bottom*). Prior flux estimates are on the left and posterior estimates on the right for each set pair of bars. Note that, except for emissions from fires, the prior flux estimates are constant for each year. Units are Tg CH_4 yr^{-1}. The total 1-σ errors for all emission categories are 15.3 Tg CH_4 yr^{-1} and 3.5 Tg CH_4 yr^{-1} for Temperate Eurasia and Temperate North America respectively.

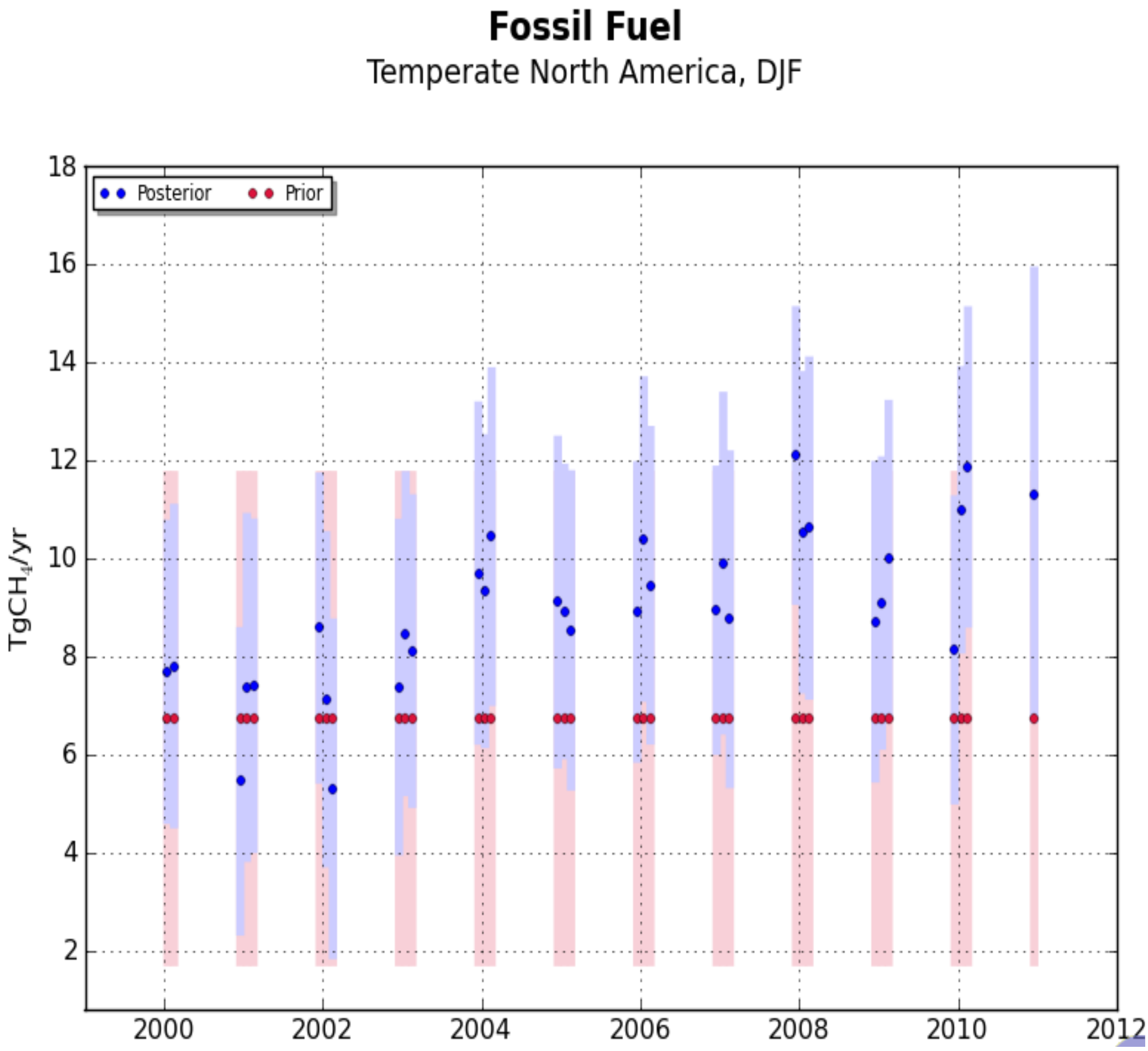

Figure 15 - Time variation of the estimated CH_4 emissions from Temperate North America for winter. Prior flux estimates are shown in red, and posterior flux estimates are shown in blue. 1-σ uncertainty bounds are shown as light red (prior) and light blue (posterior) shaded areas. Units are Tg CH_4 yr^{-1}.

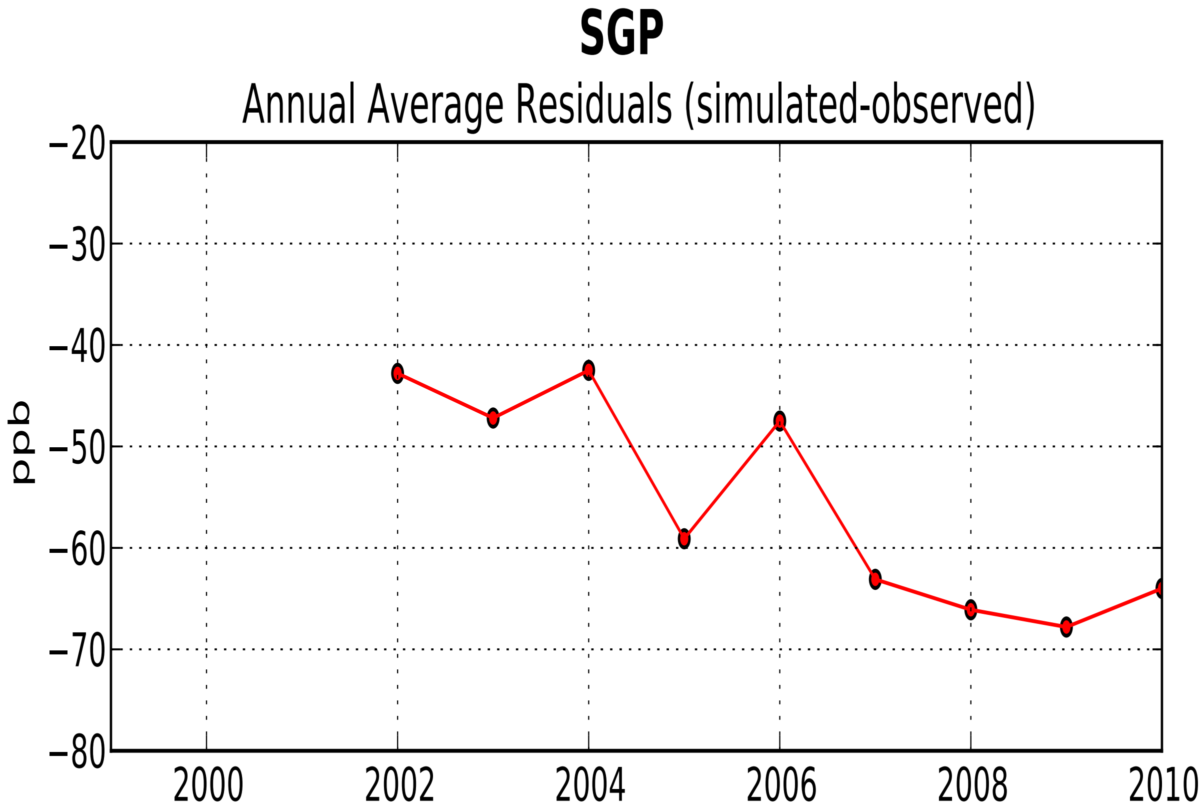

Figure 16 - Time series of residuals (the difference between the posterior and measured mole fractions). Note that the prior is constant over the length of the inversion, and the trend in the residuals can be interpreted to mean that it is increasingly difficult to fit this site over time. Units are 10^{-9} mol mol^{-1} of CH_4 (ppb).

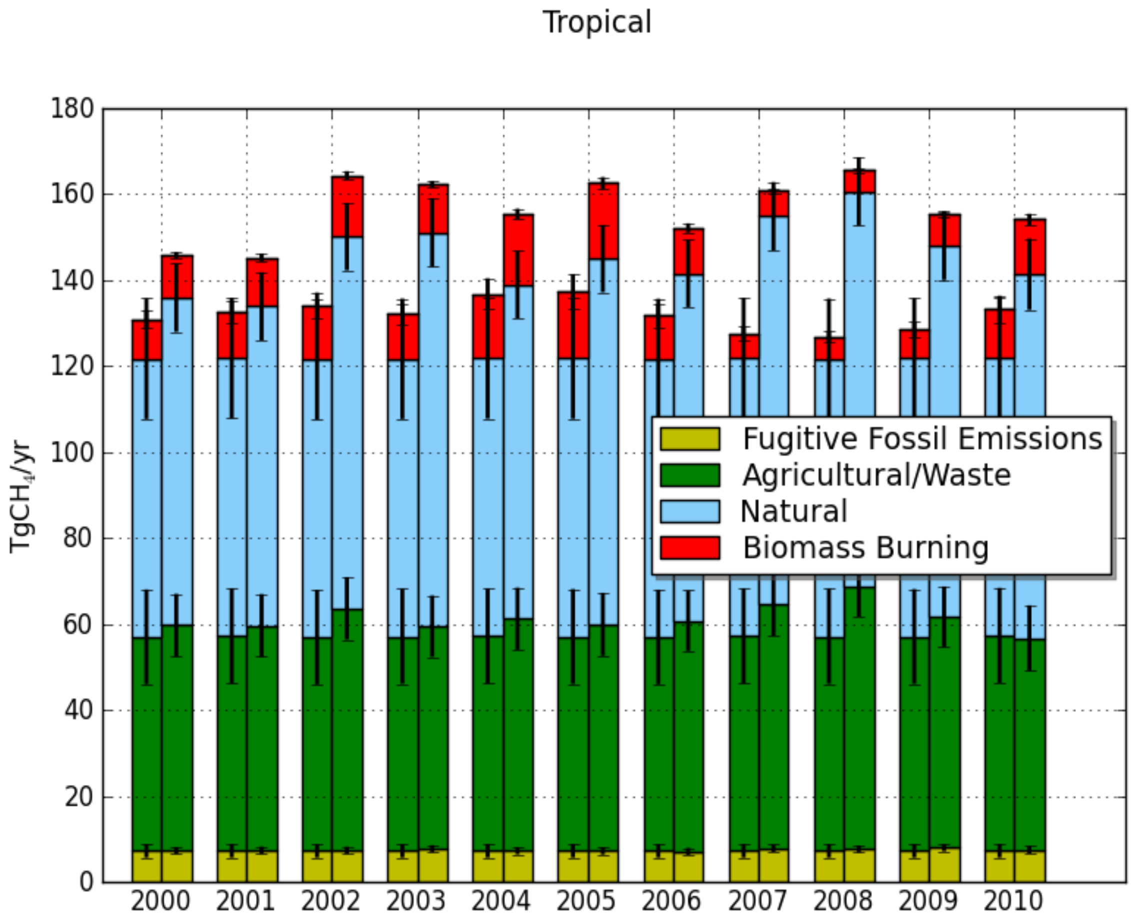

Figure 17 - The contribution to the total CH_4 flux from each category of emissions with 1-σ error bars for the Tropics (Tropical South America, Tropical Asia and Tropical Africa). For each pair of histogram bars, the prior flux estimates are shown on the left and the posterior estimates on the right. Note that, except for emissions from fires that are very small for these regions, the prior flux estimates are constant for each year. The units are Tg CH_4 yr^{-1}. The average total estimated 1-σ error is 10.8 Tg CH_4 yr^{-1}.

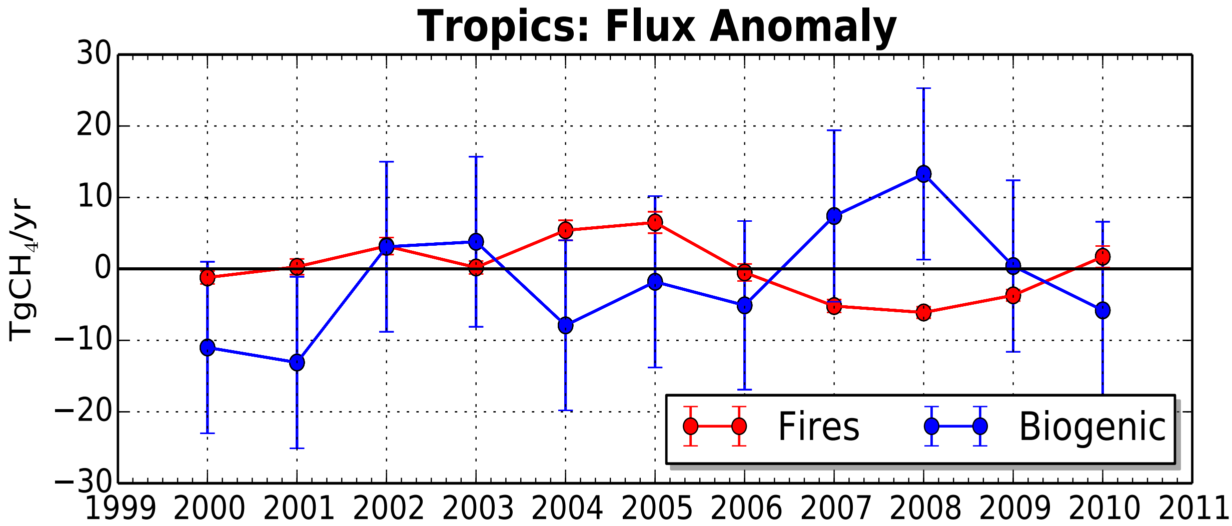

Figure 18 - Time variation of estimated total biogenic (wetlands and agriculture/waste) and fire CH_4 emission anomalies. Anomalies are calculated with respect to 10-year average posterior emissions. The units are Tg CH_4 yr^{-1}. The error bars represent 1-σ estimated error bounds on the flux anomalies.